# ELECTRICAL PROPERTIES OF SURFACES

- 5.1 The Surface Electron Potential
- 5.2 The Surface Space Charge
  - 5.2.1 The Surface Space Charge at the Solid-Vacuum Interface
  - 5.2.2 Surface Space Charge at the Solid-Liquid Interface
- 5.3 The Work Function
  - 5.3.1 Effect of Surface Roughness on Work Function
  - 5.3.2 Change of Work Function with Particle Size
- 5.4 Adsorption-Induced Charge Transfer at Surfaces: Metals and Insulators
  - 5.4.1 Charge Transfer at the Solid-Solid Interface
  - 5.4.2 Gas-Phase Ion Production by Surface Ionization: Emission of Positive and Negative Ions
- 5.5 Surface Electron Density of States
- 5.6 Electron Excitation at Surfaces
  - 5.6.1 Thermal Emission of Electrons from Surfaces
- 5.7 Electron Emission from Surfaces by Incident Electron or Photon Beams
  - 5.7.1 High-Resolution Electron-Energy-Loss Spectroscopy (HREELS)
  - 5.7.2 X-Ray Photoelectron Spectroscopy (XPS)
  - 5.7.3 Auger Electron Spectroscopy (AES)
- 5.8 Field Electron Emission
- 5.9 Field Ionization
- 5.10 Electron Tunneling
  - 5.10.1 The Scanning Tunneling Microscope (STM)
- 5.11 Summary and Concepts
- 5.12 Problems

References

#### 5.1 THE SURFACE ELECTRON POTENTIAL

The electrostatic electron potential  $V^s$  in a surface region of thickness x (the region most affected by the presence of an interface) may be divided into three parts:

$$V^{s}(x) = V_{core}(x) + V_{exchange}(x) + V_{dipole}(x)$$
 (5.1)

The  $V_{\rm core}(x)$  term represents the potential between the core electrons and valence electrons, while  $V_{\rm exchange}(x)$  is the exchange potential between the valence electrons. In the solid each electron lowers its energy by pushing the other electrons of like spin aside because of the Pauli exclusion principle (exchange interaction) or by having electrons of either spin avoid each other to minimize their repulsive (Coulomb) interaction (correlation interaction). This produces the exchange-correlation hole, a deficit of electronic charge that surrounds each electron. These potentials, along with those of the ion cores, are responsible for keeping the electrons in the solid in spite of their high concentration.  $V_{\rm core}(x)$  is not likely to change, whether the atom is at the surface or in the bulk, because of the localized nature of the core electrons. Therefore, we may neglect it for purposes of this discussion. However,  $V_{\rm exchange}(x)$  and  $V_{\rm dipole}(x)$  are very much the properties of the surface atoms.  $V_{\rm dipole}(x)$  is specific to the surface and is closely connected with the space charge that normally accumulates at the surface.

Perhaps the two most frequently measured electrical properties in surface science are the surface space charge potential  $V_{\text{dipole}}$  and the related work function  $\phi$ .

#### 5.2 THE SURFACE SPACE CHARGE

### 5.2.1 The Surface Space Charge at the Solid-Vacuum Interface

Consider an atomically smooth slab of solid in an ultrahigh-vacuum chamber. The ion cores of its atoms may be viewed as being smeared out to produce a uniform density of positive charge; electrons are bound to this uniform charge by electrostatic forces. This is the so-called jellium model that has been successful in reproducing many of the surface electrical properties of metals. At the surface the electrons are bound only toward the solid, and thus they spill out by tunneling into the vacuum, with the charge density dropping exponentially away from the surface (Figure 5.1). The electrons that accumulate on the outer edges of the solid-vacuum boundary leave a partial positive charge behind. This charge separation leads to the formation of the surface space charge. For a metal, the free-electron (those electrons that are free to hop from atom to atom in an applied potential) concentration is so high (about one electron per atom) that spatial extent of the space charge is limited to the topmost layer of atoms at the surface, since the atoms below the surface are effectively screened by the large free-electron density. For insulators or semiconductors, the

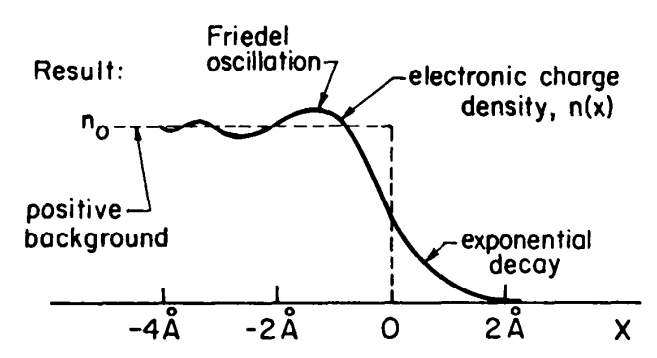


**Figure 5.1.** Schematic representation of the electronic charge density distribution at a metal surface.

space charge may extend many tens or hundreds of atomic layers into the solid, as we shall see shortly.

A more realistic model will take full account of the atomic nature of the surface and yield charge densities and electronic potentials similar to those obtained by the jellium model. In this circumstance, however, the charge density on the solid side of the surface exhibits fluctuations that are often called *Friedel oscillations* and which are due to the screening by the free electrons (Figure 5.1). The amplitude of this oscillation is a sensitive function of the electron density, as are the height and extent of the surface space-charge potential.

Both the height of the surface space-charge potential barrier  $V_s$  and its distance of penetration into the bulk d depend on the concentration of mobile charge carriers in the surface region. In order to discuss the properties of a surface space charge, let us consider an n-type semiconductor with a bulk carrier concentration  $n_e^{\text{bulk}}$ . In order to calculate the properties of the space-charge layer as a function of its charge density  $\rho_e$ , consider a homogeneous one-dimensional solid in thermal equilibrium (Figure 5.2). The potential at any point is only a function of the distance x from the surface (where x = 0) and is determined by the Poison equation:

$$\frac{d^2V}{dx^2} = -\frac{\rho_e(x)}{\epsilon\epsilon_0} \tag{5.2}$$

where  $\epsilon$  is the dielectric constant in the solid and  $\epsilon_0$  is the permittivity of free space, a constant. In our model of the space-charge layer,  $\rho_e(x) = eN_D^+$ , where  $N_D^+$  is the

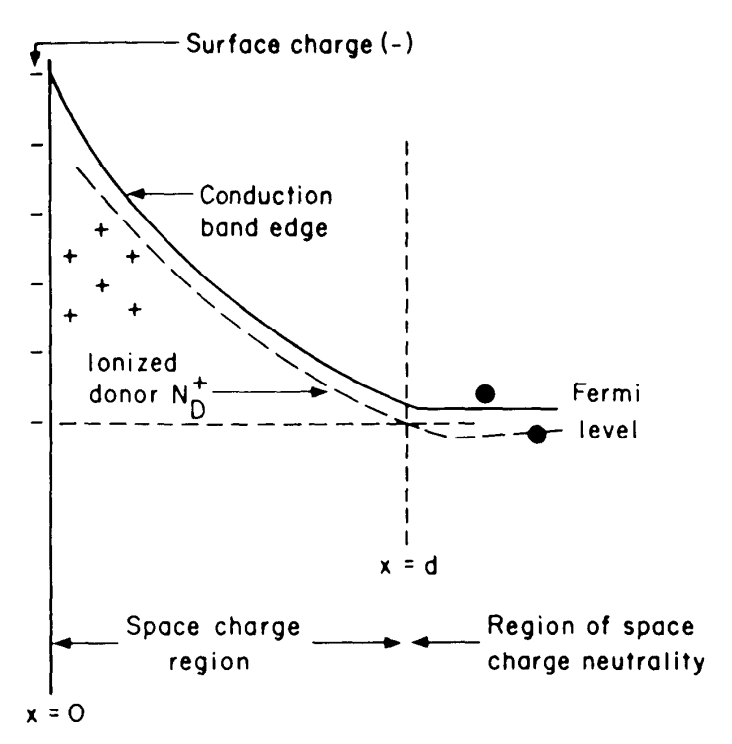


Figure 5.2. Scheme of space-charge buildup at an n-type semiconductor surface upon adsorption of electron acceptor molecules.

concentration if ionized donors. Integrating twice, one obtains

$$V(x) = -\frac{e}{2\epsilon\epsilon_0} N_D^+ (x - d)^2$$
 (5.3)

At x = d, V(x) = 0; that is, d defines the distance at which the electrostatic potential due to the charge imbalance in the space-charge layer becomes zero and the electron concentration attains its bulk value again. At the surface (x = 0),

$$V_s = \frac{e}{2\epsilon\epsilon_0} N_D^+ d^2 \tag{5.4}$$

where  $V_s$  is the height of the space-charge potential at the interface. Assuming that all the electrons of concentration  $n_e^{\text{bulk}}$  are removed from the space-charge region and trapped at the surface, leaving behind an equal static positive charge, we have

$$en_e^{\text{bulk}}d \approx eN_D^+d$$
 (5.5)

Substitution of Eq. 5.5 into Eq. 5.4 and subsequent rearrangement yield

$$d = \left[ \frac{2\epsilon \epsilon_0 V_s}{e n_e^{\text{bulk}}} \right]^{1/2} \tag{5.6}$$

This distance is called the *Debye length*. It measures the penetration depth of the electrostatic surface effects.

Thus the higher the free-carrier concentration in the material, the smaller the penetration depth of the applied field into the medium. For electron concentrations of  $10^{22}$  cm<sup>-3</sup> ( $10^{28}$  m<sup>-3</sup>) or larger, the space charge is restricted to distances on the order of one atomic layer or less, because the large free-carrier density screens the solid from the penetration of the electrostatic field caused by the charge imbalance. For most metals, almost every atom contributes one free valence electron. Because the atomic density for most solids is on the order of  $10^{22}$  cm<sup>-3</sup> ( $10^{28}$  m<sup>-3</sup>), the free-carrier concentration in metals is in the range of  $10^{20}$ – $10^{22}$  cm<sup>-3</sup> ( $10^{26}$ – $10^{28}$  m<sup>-3</sup>). Thus  $V_s$  and d are small. For semiconductors or insulators, however, typical free-carrier concentrations at room temperatures are in the range of  $10^{10}$ – $10^{16}$  cm<sup>-3</sup> ( $10^{16}$ – $10^{22}$  m<sup>-3</sup>). Therefore, at the surfaces of these materials, there is a space-charge barrier of appreciable height and penetration depth that could extend over thousands of atomic layers into the bulk. This is the reason for the sensitivity of semiconductor devices to ambient changes that affect the space-charge barrier height.

#### 5.2.2 Surface Space Charge at the Solid-Liquid Interface

So far we have only considered the properties of the surface space charge at the solid-vacuum interface. Let us now immerse the solid into a liquid. The molecules in the liquid adsorb onto the solid surface and become polarized as they respond to the electrical field at the interface to produce an electrochemical double layer. They may also line up in preferential bonding directions if they possess a permanent dipole

moment. In this circumstance an electrical field is induced on the liquid side of the solid-liquid interface, with marked consequences for molecule transport or charge transport to and from the interface. The charge layer that forms on the liquid side of the solid-liquid interface is often called the *Helmholtz layer*, and it plays an important role in affecting electrochemical changes associated with reduction or oxidation of charged species when the solid is used as an electrode.

The presence of charged species at the solid-liquid interface helps to stabilize colloids. These are small particles,  $10^4-10^5$  Å ( $10^3-10^4$  nm) in diameter, that carry the same charge and thus exhibit repulsive electrostatic interaction. Because all particles in a colloid system are of the same size, they are thermodynamically stable because their solubilities (or vapor pressures) are the same according to the Kelvin equation. Their surface charge provides extra stability because of the strong repulsion. Milk, blood, paint, and latex are examples of important colloid systems in biology and in the chemical technologies. Mechanical agitation can strip off the charged protein coating of a milk colloid, causing coagulation (whipping cream). The elimination of the repulsive charge by other means (adsorption or drying) can readily destabilize these systems. One important application of the surface space charge is copying in xerography. In this process a charged organic or inorganic insulator is selectively illuminated by using the mirror reflection of the printed page, thereby removing the charge only at the illuminated sites. By pressing an insulating surface (paper) against the charged surface, its charge is transferred and is then fixed by colored polymer particles that melt when heated at their sites of adsorption (that is, where the charges were on the paper).

#### 5.3 THE WORK FUNCTION

The work function is defined as the minimum potential the most loosely bound valence electrons in the solid must overcome in order to be ejected into the vacuum outside the solid with zero kinetic energy at absolute zero temperature. A schematic energy-level diagram showing the work function, using the free-electron gas model of a metal, is depicted in Figure 5.3. The potential energy of the electrons at the top of the valence band is often called the Fermi energy  $E_F$ . Thus the work function can be defined as

$$e\phi = eV_{\text{exchange}} + eV_{\text{dipole}} - E_F \tag{5.7}$$

where  $V_{\rm exchange}$  is a bulk property that depends on the bulk electron density. The term  $V_{\rm dipole}$  is due to the surface space-charge potential that must be overcome by the electrons in the solid in order to exit into the vacuum. The term  $V_{\rm dipole}$  is responsible

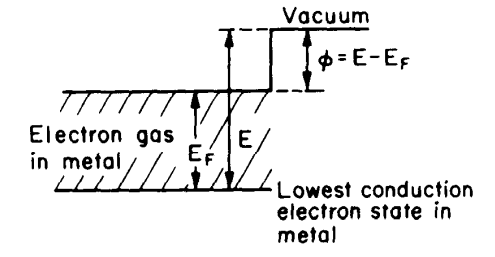


Figure 5.3. Energy level diagram to define the work function.

Crystal Face	Work Function						
	Tungsten (ref. 1)		Molybdenum (ref. 2)		Tantalum (ref. 2)		
	eV	10 <sup>-19</sup> J	eV	10 <sup>-19</sup> J	eV	10-19	
(110)	4.68	7.50	5.00	8.01	4.80	7.69	
(112)	4.69	7.51	4.55	7.29	_	_	
(111)	4.39	7.03	4.10	6.57	4.00	6.41	
(001)	4.56	7.31	4.40	7.05	4.15	6.65	
(116)	4.39	7.03					

TABLE 5.1. Work Functions Measured from Different Crystal Faces of Tungsten, Molybdenum, and Tantalum

#### REFERENCES

- M. Kaminsky, Atomic and Ionic Impact Phenomena on Metal Surfaces. Academic Press, New York, 1965.
- 2. O.D. Protopopov et al. Sov. Phys. Solid State (English translation), 8:909 (1966).

for having each crystal surface exhibit a different work function. The work functions measured for various crystal faces of several metals are listed in Table 5.1. Calculations using the jellium model result in work functions very similar to those listed in Table 5.1.

#### 5.3.1 Effect of Surface Roughness on Work Function

As the atomic density at the surface decreases, it becomes rougher on the atomic scale. The valence electrons spill out into the vacuum as before, but they smooth out the roughness in the positive charge distribution. The result is an electrostatic dipole oriented opposite to the spill-out dipole. As a consequence, the net dipole is reduced relative to its value at the higher-atomic-density, smoother surface, yielding a lower work function.

Changes in work function with increasing step density (roughness) are shown for stepped platinum and gold surfaces in Figure 5.4. As can be seen, the work function decreases linearly with increasing step density. The induced dipole moment  $\mu$  due to steps can be calculated from the work-function change because  $\Delta \phi = 4\pi N_s \mu$ , where  $N_s$  is the step density. In Figure 5.4, note that platinum has a steeper slope for the work-function change with step density than does gold, indicating a larger dipole per step atom (0.6 Debye per step atom =  $2 \times 10^{-30} \, \text{C} \cdot \text{m}$  per step atom) than on the gold stepped surface (0.27 Debye per step atom =  $0.9 \times 10^{-30} \, \text{C} \cdot \text{m}$  per step atom). A step site on a tungsten surface has a 0.30-Debye dipole on the average, while at a tungsten adatom on the surface there is a dipole moment as large as 1.0 Debye,  $3.3 \times 10^{-30} \, \text{C} \cdot \text{m}$ ).

#### 5.3.2 Change of Work Function with Particle Size

The work function of a solid is equivalent to its ionization potential. It is always lower than the ionization potential of the single atoms that make up the solid.\* These

<sup>\*</sup>This is because the remaining electrons partially screen the positively charged "hole" left behind.

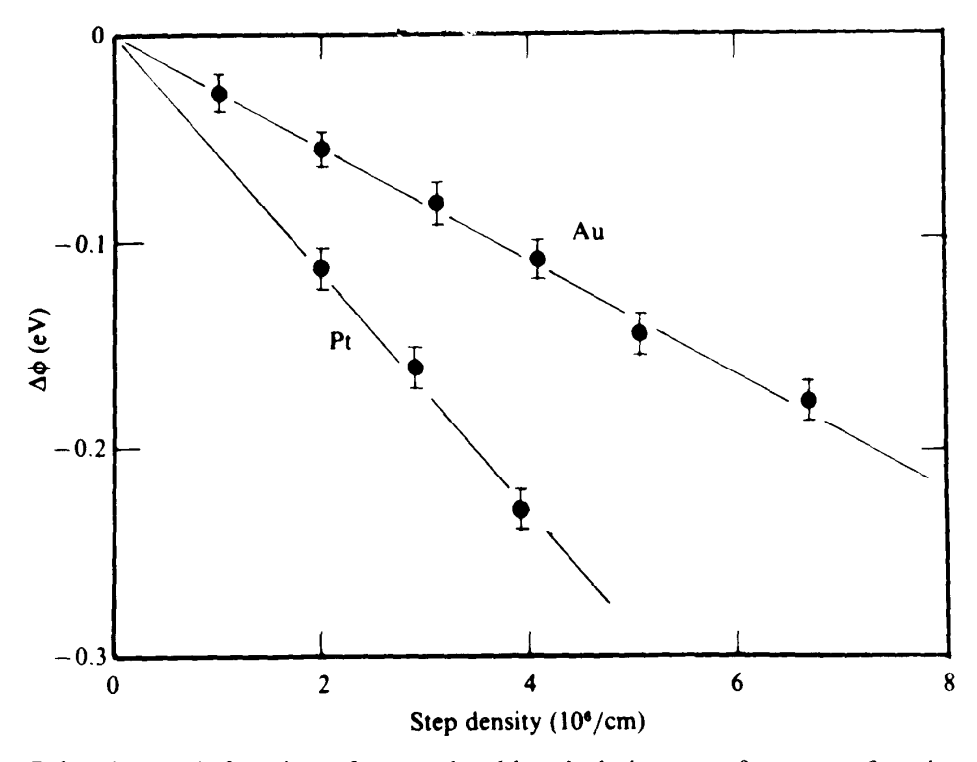


Figure 5.4. The work function of stepped gold and platinum surfaces as a function of step density (roughness) [6, 52].

values are listed for alkali atoms and solids in Table 5.2. It is important to find out how the single-atom ionization potential approaches the value of the work function as the atoms aggregate into clusters. It might even be possible to determine the ionization potential of clusters of ever-increasing size. Such experiments are in progress in several laboratories. By producing atom clusters of different sizes by laser evaporation or by ion bombardment, the ionization threshold of these clusters can then be probed using photoionization and employing variable photon energies. At present, the existing data indicate that the ionization potential decreases with increasing particle size in an oscillatory manner rather than smoothly [1]. This effect is shown for iron clusters in Figure 5.5. Whether these variations are due to changes in cluster structure or to other effects will have to be elucidated by future studies.

TABLE 5.2. Work Functions and Ionization Potentials of Alkali Metals<sup>a</sup>

Element	Work Function		Ionization Potential		
	φ (eV)	$\phi (10^{-19} \times \text{J/mole})$	$V_{\rm ion}$ (eV)	$V_{\rm ion} (10^{-19} \times {\rm J/mole})$	
Lithium	2.9	4.6	5.392	8.639	
Sodium	2.75	4.41	5.139	8.234	
Potassium	2.30	3.69	4.341	6.955	
Rubidium	2.16	3.46	4.177	6.692	
Cesium	1.81	3.03	3.894	6.239	

<sup>&</sup>quot;Data from CRC Handbook of Chemistry and Physics, 64th edition. CRC Press, Boca Raton, FL, 1983.

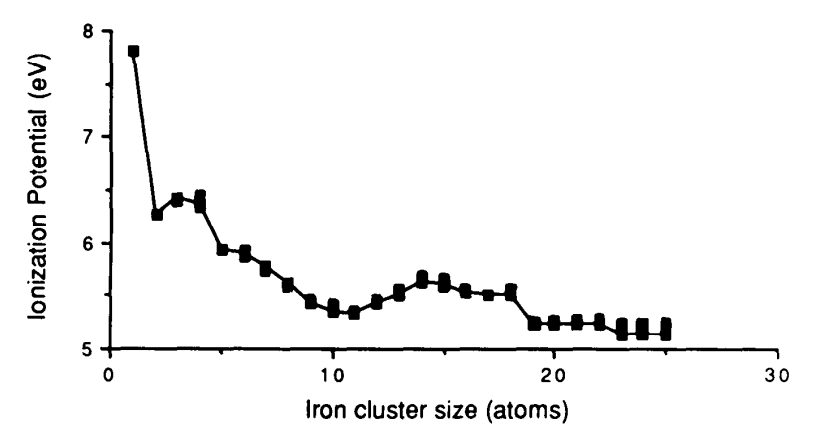


Figure 5.5. The ionization potential for iron clusters as a function of cluster size [1].

# 5.4 ADSORPTION-INDUCED CHARGE TRANSFER AT SURFACES: METALS AND INSULATORS

The surface space charge or surface dipole presents an electric field that influences atoms or molecules that may adsorb. Even inert gas atoms such as argon or xenon respond to this field upon adsorption because of their polarizability. The magnitude of the polarizability depends on the volume occupied by the electrons, and it increases with increasing atomic volume. The charge distribution of these atoms will be modified slightly in a way that lowers the work function of the adsorbing metal. Typical values of metal-work-function changes upon adsorption of a monolayer of inert gas atoms are shown in Table 5.3. The work-function change is also site-dependent, as shown for xenon at a stepped Pd(810) surface in Figure 5.6. Because the work-function change upon adsorption is greater at steps, it provides information about surface structure. Changes in work function can often be calibrated to monitor the coverage of adsorbates. The relationship between work function and surface composition is complicated, however, because of the adsorbate-adsorbate interaction, which also influences adsorption-induced changes of the surface dipole.

The opposite situation from weak interaction of inert gases with the surface space charge is surface ionization, when the adsorbate is ionized by the substrate. This typically occurs in alkali-metal adsorption on transition-metal surfaces. In the more usual situation with chemisorbed molecules, only partial charge transfer occurs to or from the substrate to the molecule. If the negative pole of the molecule points toward the vacuum, the induced electric fields cause an increase in the work function. Table 5.4 lists the work-function changes obtained by the chemisorption of several molecules on rhodium.

Let us discuss the model that is commonly used to interpret the chemisorptioninduced changes in work function, along with some of the experimental results.

Chemisorption of an atom or a molecule leads to charge transfer to or from the metal. This charge transfer is larger than it is for inert gas adsorption. The charge transfer results in a larger change of work function, with the magnitude of the change depending on the nature of the adsorbate-substrate bond and on the coverage. If we consider well-separated chemisorbed species with surface concentration  $\sigma$  and po-

TABLE 5.3. Sign of Work-Function Change,  $\Delta \phi$ , Upon Adsorption at 300 K

System	Sign of Work-Function Change, $\Delta \phi$	Reference
O/Ag(111)	Positive	1
O/Cu(100)	Positive	2
O/Cu(110)	Positive	2
O/Cu(111)	Positive	2 2 3
O/Ni(110)	Positive	3
CO/Cu(100)	Negative	4
CO/Mn	Positive	5
CO/Ni(111)	Positive	6
H/Mo(001)	Positive	7
H/Mo(011)	Positive	7
H/Mo(111)	Positive	7
H/Ni(110)	Positive	8
H/W(100)	Positive	9
Cs/Ni(100)	Negative	10
Cs/W(100)	Negative	11
K/Ni(110)	Negative	12
Xe/Pd(100)	Negative	13
Substitute / Pt(111)	Negative	14
Aromatic molecules / Pt(100)	Negative	12
Cl/W(100)	Positive	15
Cl/ <sub>B</sub> Ti	Positive	16
Ba/W(100)	Negative	17
$CH_4/W(110)$	Positive	18
Na/W(110)	Negative	19
Li/W(110)	Negative	20

#### REFERENCES

- 1. A.W. Dweydari and C.B.H. Mee. Phys. Status Solidi A 17:247 (1973).
- 2. T.A. Delchar. Surf. Sci. 27:11 (1971).
- 3. J. Küppers. Vacuum 21:393 (1971).
- 4. J.C. Tracy. J. Chem. Phys. 56:2748 (1972).
- 5. G.H. Hall and C.H.B. Mee. Phys. Status Solidi A 12:509 (1972).
- 6. K. Christmann, Ol Schober, and G. Ertl. J. Chem. Phys. 60:4719 (1974).
- 7. E. Chrzanowski. Acta Phys. Pol. A44:711 (1973).
- 8. T.N. Taylor and P. J. Estrup. J. Vacuum Sci. Technol. 11:244 (1974).
- 9. C.A. Papageorgopoulos and J.M. Chen. Surf. Sci. 39:283 (1973).
- 10. C.A. Papageorgopoulos and J.M. Chen. Surf. Sci. 52:40 (1975).
- 11. T.J. Lee, B.H. Blott, and B.J. Hopkins. J. Phys. F 1:309 (1971).
- 12. R.L. Gerlach and T.N. Rhodin. Surf. Sci. 19:403 (1970).
- 13. P.W. Palmberg. Surf. Sci. 25:598 (1971).
- 14. J.L. Gland and G.A. Somorjai. Surf. Sci. 41:387 (1974).
- 15. D.L. Fehrs. Surf. Sci. 17:298 (1969).
- 16. J.R. Anderson and N. Thompson. Surf. Sci. 28:84 (1971).
- 17. Yu.S. Vedula, Yu.M. Konoplev, V.K. Medvedev, A.G. Naumovets, T.P. Smereka, and A.G. Fedorous. *Materials of the 3rd International Conference on Thermionic Electrical Power Generation*, Jülich, Germany 1972.
- 18. S. Hellwig and J.H. Block. Surf. Sci. 19:523 (1972).
- 19. E.V. Klimenko and V.K. Medvedev. Sov. Phys. Solid State 10:1562 (1969); Fiz. Tverd. Tela 10:1986 (1968).
- 20. V.K. Medvedev and T.P. Smereka. Sov. Phys. Sol. Stat. 16:1046 (1974); Fiz. Tverd. Tela 16:1599 (1974).

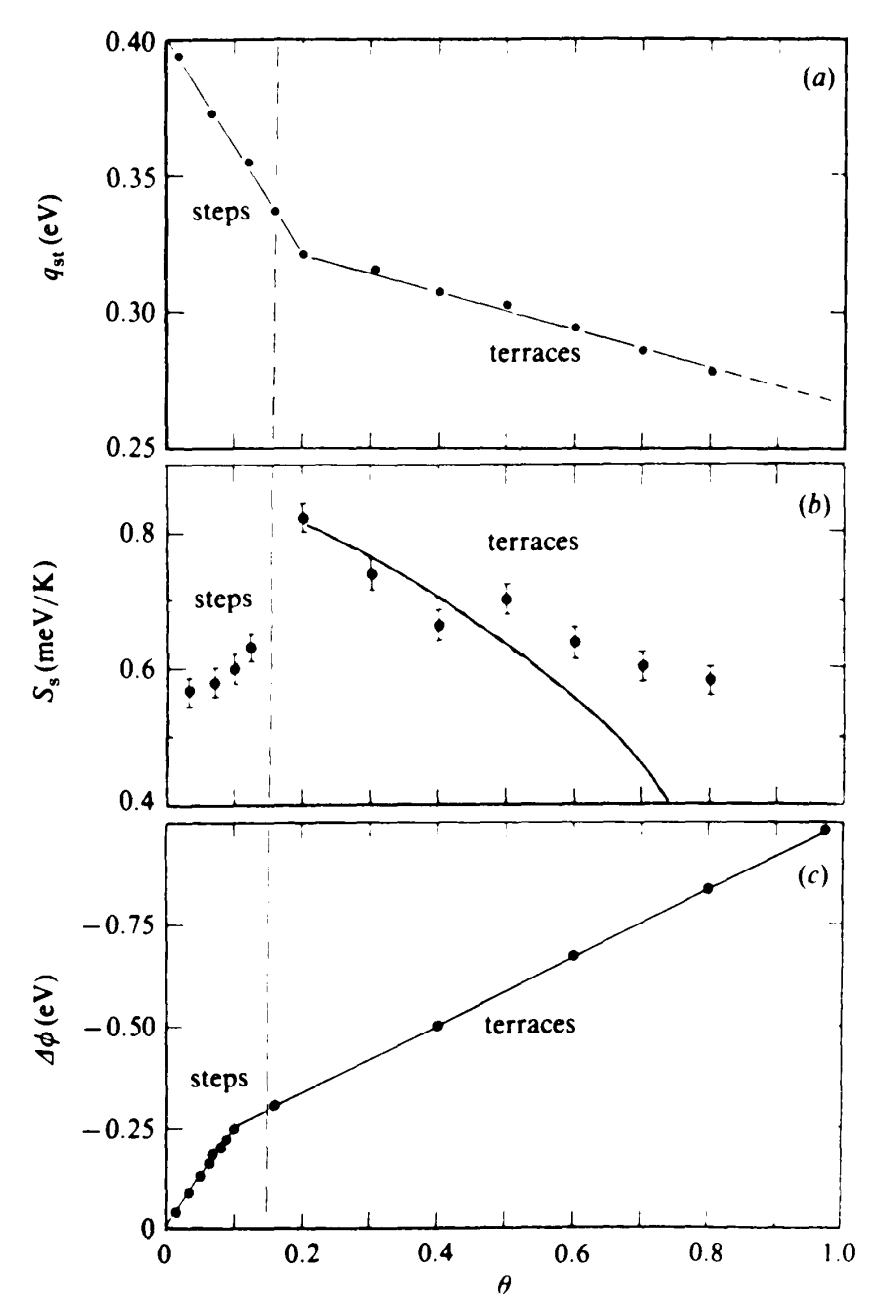


Figure 5.6. The enthalpy change (a), the entropy (b), and the work function change (c) for xenon adsorption as a function of xenon coverage on the Pd(810) stepped crystal surface [53].

larizability  $\alpha$ , then the work-function change  $\Delta \phi$  is given by the Helmholtz equation:

$$\Delta \phi = 4\pi e \mu \sigma \tag{5.8}$$

where  $\mu$  is the dipole moment induced by the adsorbate that localizes a fraction of the surface space charge in the form of a charge density that screens the field due to the charged adsorbate. This screening charge and the charge on the adsorbate form a dipole  $\mu = qa$ , where a is the separation between the adsorbate and the screening

	Number of CO Molecules per Coadsorbate						
Coadsorbate	0	1	2				
$C_6D_6$	$(2\sqrt{3}\times3)$ rect	$c(2\sqrt{3}\times4)$ rect	$(3 \times 3)$				
V V	-1.36  eV	−0.64 eV	-0.26 eV				
	$-2.18 \times 10^{-19} \mathrm{J}$	$-1.03 \times 10^{-19} \mathrm{J}$	$-0.42 \times 10^{-19} \mathrm{J}$				
$C_6D_5F$	$(\sqrt{19} \times \sqrt{19})R23.4^{\circ}$	$c(2\sqrt{3}\times4)$ rect	$(3 \times 3)$				
V.	-1.24  eV	−0.61 eV	−0.24 eV				
	$-1.99 \times 10^{-19} \mathrm{J}$	$-0.98 \times 10^{-19} \mathrm{J}$	$-0.38 \times 10^{-19} \mathrm{J}$				
$\equiv$ CCH <sub>3</sub>	Disordered	$c(4 \times 2)$	_				
v	-1.23 eV	-0.32  eV	_				
	$-1.97 \times 10^{-19} \mathrm{J}$	$-0.51 \times 10^{-19} \mathrm{J}$					

TABLE 5.4. Work-Function Changes Relative to the Clean Rh(111) Surface for Various Ordered Structures, with and without Coadsorbed CO

charge and q is the unit charge. Equation 5.8 can be written as

$$\Delta \phi = -3.76 \times 10^{-5} \mu \sigma \tag{5.9}$$

where  $\Delta \phi$  is in eV,  $\mu$  is in Debyes, and N is the number of adsorbate atoms per cm<sup>2</sup>. Dipoles of like orientation cause depolarization, which shows up at higher coverages that modify the Helmholtz equation according to the point-depolarization model developed by Topping:

$$\Delta\phi = -\frac{4\pi e\mu\sigma}{1 + 9\alpha\sigma^{3/2}}\tag{5.10}$$

where  $\mu$  is the initial dipole moment observed at low coverages and  $\alpha$  is the polarizability. Equation 5.10 is given in SI units by

$$\Delta \phi = -\frac{e\sigma\mu}{\epsilon_0 \left[1 + \left(\frac{9}{4\pi}\right)\alpha\sigma^{3/2}\right]}$$
 (5.11)

where  $\epsilon_0$  is the vacuum permittivity.

Carbon monoxide increases the work function of rhodium upon chemisorption. Figure 5.7 shows the work-function change as a function of coverage  $\theta$ . A good fit can be obtained for  $\theta \le 0.33$  (shown by the dashed curve in Figure 5.7) with  $\mu_{CO} = -0.2$  Debye  $(-0.67 \times 10^{-30} \, \text{C} \cdot \text{m})$  and  $\alpha_{CO} = 0.34 \times 10^{-28} \, \text{m}^3$ .

For  $\theta_{\rm CO} > 0.33$ ,  $\Delta \phi$  increases dramatically until reaching a value of +1.05 eV  $(1.7 \times 10^{-19} \, \rm J)$  and  $\theta_{\rm CO} = 0.75$ , which is near the saturation coverage. Above  $\theta_{\rm CO} = 0.33$ , the CO molecules begin to occupy bridge sites (bridging two rhodium atoms) in addition to top sites. The large increase of  $\Delta \phi$  above one-third monolayer coverage is attributed to the fact that bridge-bonded CO has a larger surface-dipole moment than does top-site-bonded CO. Thus, changes in bonding that occur with changes in surface concentration have a strong effect on the work-function change.

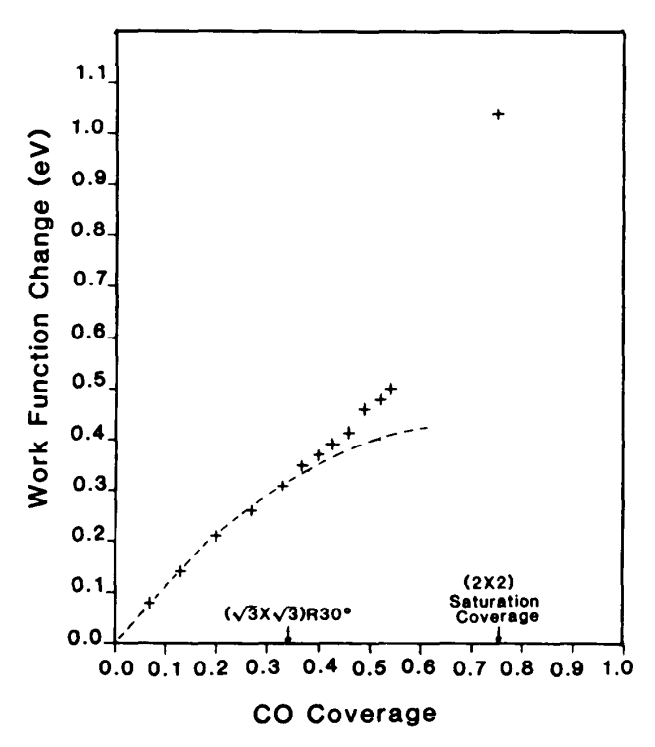


Figure 5.7. The change of work function of Rh(111) upon CO adsorption as a function of coverage [54].

Figure 5.8 shows the work-function change as associated with sodium chemisorption on the (111) crystal face of rhodium. The 5.4-eV (8.7  $\times$  10<sup>-19</sup>-J) work function of the transition metal decreases rapidly to 2.5 eV at  $\theta_{\rm Na} \approx 0.2$ . Using Eq. 5.11, we obtain a surface-dipole moment of  $\mu_{\rm Na} = +5.1$  Debye (1.7  $\times$  10<sup>-30</sup> C · m) and polarizability  $\alpha_{\rm Na} = 2.9 \times 10^{-28}$  m³ for low sodium coverages. Similar values have been observed for the chemisorption of alkali adatoms on other transition -metal surfaces as well.

The large charge transfer and the high heat of adsorption [  $\approx$  60 kcal/mole (  $\approx$  251 kJ/mole)] associated with the initial stages of alkali-metal chemisorption indicate ionization of the alkali atoms. At higher coverages of alkali metal, however, further work-function change becomes minimal, and the heat of adsorption declines to that of the heat of sublimation of sodium [23 kcal/mole (96 kJ/mole)]. Detailed surface studies on several alkali-metal-transition-metal systems reveal that, at above 20% coverage, the repulsive interaction between the dipoles created by the presence of the alkali ions leads to depolarization and neutralization until a metallic alkali atomic layer is produced.

The chemisorption of organic molecules on transition metals usually reduces their work function. According to the available experimental data, the chemisorption of ethylene in the form of ethylidyne reduces the work function by about -1.2 eV  $(-1.9 \times 10^{-19} \text{ J})$ , corresponding to the formation of a surface dipole of +0.9 Debye  $(3 \times 10^{-30} \text{ C} \cdot \text{m})$ . Benzene chemisorption reduces the work function by -1.4 eV  $(-2.2 \times 10^{-19} \text{ J})$ , corresponding to a dipole of (+2.0 Debye)  $(6.7 \times 10^{-30} \text{ C} \cdot \text{m})$ .

Gas adsorption on insulator or semiconductor surfaces can cause very large changes in the height of the surface space-charge potential and its Debye length. As

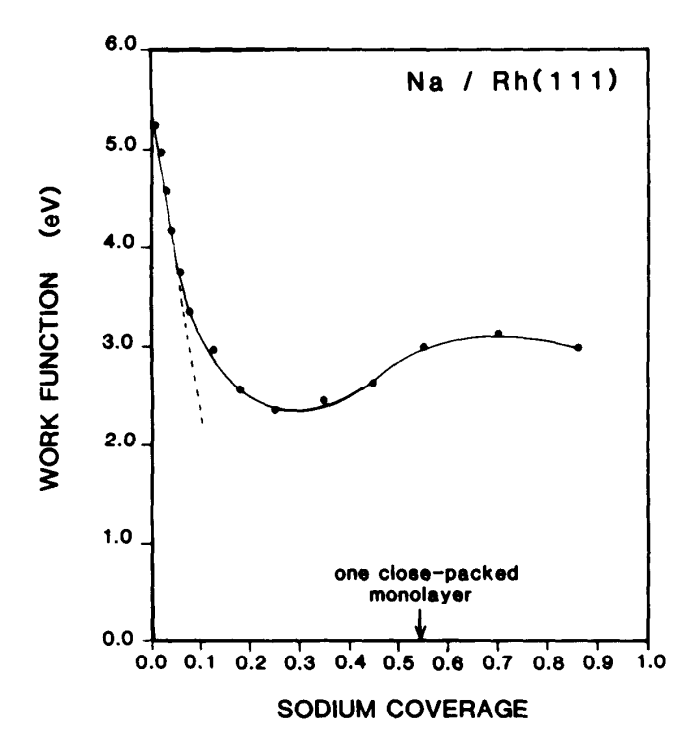


Figure 5.8. The change of work function of Rh(111) upon adsorption of sodium as a function of Na coverage [54].

a result, when used as thin-film adsorbers, the electrical conductivity of these surfaces can be markedly altered. This effect provides a way to detect minute amounts of gases or vapors, such as methane in coal mines or smoke induced by fires. Tin oxide (SnO<sub>2</sub>) appears to be the semiconductor of choice for many gas-sensor applications because of its chemical resilience [2, 3]. The thickness of the SnO<sub>2</sub> film controls its sensitivity to adsorbates by adsorption-induced charge transfer, which shows up in changes in electrical conductivity.

The co-deposition of transition metals can enhance chemical reactivity and further increase the sensitivity of the semiconductor detectors. Chemisorption-induced changes in surface electrical properties promise to be important in the chemical analysis of blood and in other biochemical applications.

Adsorption-induced charge transfer also markedly influences the heat of adsorption. A molecule that transfers more charges to or from a surface adsorbs more strongly. This gives rise to the possibility of separating mixtures of molecules (gases or liquids) by virtue of stronger adsorption of those with larger charge transfer. Usually molecules with lower ionization potentials or larger electron affinities are likely to transfer more charge and thus are likely to adsorb more strongly. The rate of charge transfer  $dn_s/dt$  to or from the molecule is related to the height of the surface space charge  $V_s$ , because the electrons must flow over the top of the potential energy barrier:

$$\frac{dn_s}{dt} \approx \exp\left(-\frac{eV_s}{k_B T}\right) \tag{5.12}$$

Because  $V_s$  is proportional to  $n_s^2$  (assuming a parabolic drop-off of the surface

barrier height toward the bulk), the rate of charge transfer can be expressed as

$$\frac{dn_s}{dt} \approx \exp\left(-n_s^2\right) \tag{5.13}$$

This type of rate law frequently describes the adsorption of oxygen on semiconductor surfaces and gives straight-line plots of current versus logarithm of time.

The magnitude of charge transfer may be one electron per  $10^2$  adsorbed molecules; nevertheless, even this magnitude leads to the preferential adsorption of  $O_2$  from air (an  $N_2$ - $O_2$  mixture) because oxygen forms stronger charge-transfer bonds than does nitrogen. On surfaces that do not exhibit charge transfer (microporous alumina-silicate molecular sieves, for example),  $N_2$  would adsorb more strongly than  $O_2$  because of its larger polarizability.

### 5.4.1 Charge Transfer at the Solid-Solid Interface

When two different metal surfaces are brought into contact, the surface space charges that were present at their interfaces with a vacuum will be modified. The electrons from the metal of lower work function will flow into the other metal until an interface potential develops that opposes further electron flow. This is called the *contact potential* and is related to the work-function difference of the two metals. The contact potential depends not only on the materials that make up the solid-solid interface but also on the temperature. This temperature dependence is used in thermocouple applications, where the reference junction is held at one temperature while the other junction is in contact with the sample. The temperature difference induces a potential (called the *Seebeck effect*), because of electron flow from the hot to the cold junction, that can be calibrated to measure the temperature. Conversely, the application of an external potential between the two junctions can give rise to a temperature difference (Peltier effect) that can be used for heat removal (refrigeration).

Metal-semiconductor contacts play important roles in the technologies of electronic circuitry. Because electrons flow from the material with the lower work function to the material with the higher work function, a blocking contact (Schottky barrier) is produced that inhibits the further flow of electrons in one direction while aiding the flow of electrons in the other direction. Often, however, ohmic metal-semiconductor contacts are needed that permit charge transport across the interface in both directions without a barrier. This can often be accomplished by forming interface compounds between the metal and the semiconductor that can eliminate the formation of the interface space charge. For silicon technology, nickel or cobalt silicides can serve as ohmic contacts between the metal and the semiconductor.

Recently, work-function changes at semiconductor-metal interfaces have been used to image the oxide-metal interface on the atomic scale by using the scanning tunneling microscope (STM). Figure 5.9 shows a picture of the  $TiO_2$ -Rh system prepared by depositing titanium oxide islands on the transition-metal surface. The tunnel current I in the STM varies exponentially with both work function  $\phi$  and distance d:  $I \approx \exp{(-\phi d/2)}$ . By periodically changing the tunneling tip-surface distance by oscillating the tip, the derivative dI/dd can be measured; this derivative is proportional to the barrier height, which is related to  $\phi$ . In this way an atomic resolution of the structure of oxide-metal interfaces can be obtained.

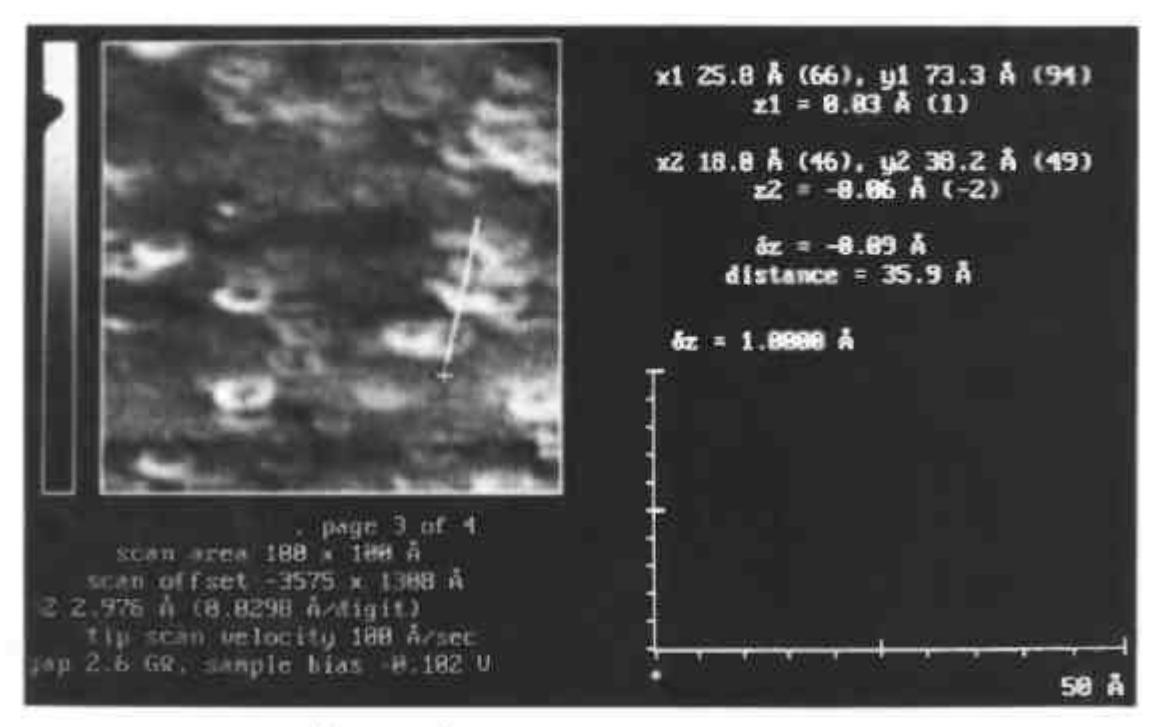


Figure 5.9. A 100 Å × 100 Å STM image of 0.9 monolayer of TiO2 on rhodium.

# 5.4.2 Gas-Phase Ion Production by Surface Ionization: Emission of Positive and Negative Ions

Consider an atom of ionization potential  $V_{\rm ion}$  adsorbed on a metal surface of work function  $\phi$ . If the atom is in thermal equilibrium with the solid, it may vaporize as a neutral atom from the surface after acquiring thermal energy equal to its heat of desorption from the metal  $\Delta E_{\rm des}$ . The desorption energy  $\Delta E_{\rm des}^+$  necessary to vaporize it as a positive ion, on the other hand, can be estimated by [4]

$$\Delta E_{\text{des}}^{+} \approx \Delta E_{\text{des}} + V_{\text{ion}} - \phi$$
 (5.14)

The value of  $\Delta E_{\rm des}^+$  is obtained by summing the energies needed to vaporize a neutral atom, ionize it in the vapor phase, and then return the electron to the metal surface. If  $V_{\rm ion} - \phi$  is positive, the surface atoms are likely to desorb as neutral species, since  $\Delta E_{\rm des} \leq \Delta E_{\rm des}^+$ . However, for systems in which the metal work function is greater than the ionization potential of the adsorbing atom (i.e., if  $V_{\rm ion} - \phi \leq 0$ ), the vaporization of ionic species will occur preferentially. Thus, for studies of surface ionization, high-work-function metals (W, Pt) and adsorbates with low ionization potentials (Cs, Rb, K) are used.

The degree of ionization—the ratio of ion flux  $j_+$  to the flux of neutral atoms  $j_0$  desorbing from the metal surface—is given by the Saha-Langmuir equation [5]:

$$\frac{j_{+}}{j_{0}} = \frac{g_{+}}{g_{0}} \exp \left[ -\frac{e(V_{\text{ion}} - \phi)}{k_{B}T} \right]$$
 (5.15)

	Li	Na	K	Rb	Cs
	$(V_{\rm ion} =$	$(V_{\rm ion} =$	$(V_{\rm ion} =$	$(V_{\rm ion} =$	$(V_{\rm ion} =$
	5.40  eV =	5.12  eV =	4.32  eV =	4.10  eV =	3.88  eV =
T(K)	$8.65 \times 10^{-19} \mathrm{J})$	$8.20 \times 10^{-19} \text{ J}$	$6.92 \times 10^{-19} \mathrm{J})$	$6.57 \times 10^{-19} \text{ J}$	$6.22 \times 10^{-19} \mathrm{J})$
1000	$1.8 \times 10^{-5}$	$5.0 \times 10^{-4}$	6.3	103.9	790.0
1500	$5.5 \times 10^{-4}$	$5.0 \times 10^{-3}$	2.2	35.8	72.0
2000	$3.0 \times 10^{-3}$	$1.5 \times 10^{-2}$	1.6	11.4	19.9
2500	$8.4 \times 10^{-3}$	$3.2 \times 10^{-2}$	1.3	7.0	9.8

TABLE 5.5. Calculated Values for the Degree of Ionization for Different Alkali Metals on a Tungsten Surface at Different Temperatures

where  $g_+/g_0$  is the ratio of the statistical weights of the ionic and atomic states. Table 5.5 shows the calculated values for the degree of ionization for different alkali metals on a tungsten surface at different temperatures. We can see that elements with small ionization potentials (Cs and Rb) yield predominantly ion fluxes, while for elements with large ionization potentials, such as lithium and sodium fluxes, the neutral species predominate.

Equation 5.15 has been verified by experiments using several different metal surfaces. Deviations from the predicted ion flux are due to the presence of impurities on the metal surface that may change its work function, and the fact that thermal equilibrium may not be completely established between the adsorbate and the surface within its residence time on the metal [4]. This latter effect can give rise to a partial reflection of the incident vapor atoms as neutral species, thereby reducing the ion flux to below a value predicted by Eq. 5.15. The surface temperature in surface-ionization experiments should be high enough so that thermal desorption of the adsorbed species can take place rapidly. Otherwise, accumulation of the adsorbate on the surface would impede the surface-ionization reaction by reducing the concentration of surface sites on which ionization can take place and by decreasing the work function of the clean surface.

Because a metal surface is heterogeneous, there are local variations of the work function along the crystal surface. For a polycrystalline substrate that exposes many crystal faces, the work function changes from crystal face to crystal face. Therefore, it is advantageous in surface-ionization experiments to establish conditions that allow surface diffusion of the adsorbed species to occur. In this way the ionization probability may be increased.

Alkali metals are not the only alkali species that have been ionized by surface ionization. Alkali halides (NaCl, LiF, etc.) and alkali-earth metal atoms (Ba, Mg, etc.) have also been ionized by this method. Tungsten and platinum surfaces are used most frequently in these studies.

The emission of negative ions has also been observed under conditions of surface ionization. If the electron affinity  $S_e$  of a negative ion is defined by the reaction  $A^- \to A + e$ , the desorption energy of negative ions,  $\Delta E_{\rm des}^-$  can be estimated by [4]

$$\Delta E_{\rm des}^- \approx \Delta E_{\rm des} - S_e + \phi \tag{5.16}$$

Here we form the negative ion by vaporizing a neutral atom and an electron from the surface and then combining them in the vapor. The electron affinities of several

1 Obline Values						
	F	Cl	Br	I	0	S
Electron affinity (eV):	3.6	3.7	3.5	3.2	3.1	2.4
Electron affinity (10 <sup>-19</sup> J):	5 77	5 03	5.61	5.13	(2.3) 4.97	3.85
Election annity (10 3).	5.11	3.93	5.01	3.13	(3.69)	3.63

TABLE 5.6. Electron Affinities of Several Elements Which Exhibit the Largest Positive Values

elements that exhibit the largest positive values of  $S_e$  are shown in Table 5.6. For many elements, however, the electron affinity is negative; these elements are not likely candidates for negative surface ionization. If  $(S_e - \phi) > 0$ —that is, if the electron affinity is greater than the work function (which is always positive)—the atoms adsorbed on the metal surface are most likely to desorb as negative ions. The degree of ionization is given by

$$\frac{j_{-}}{j_{0}} = \frac{g_{-}}{g_{0}} \exp\left[-\frac{e(-S_{e} + \phi)}{k_{B}T}\right]$$
 (5.17)

which is similar to Eq. 5.15. Negative-ion emission requires metal surfaces with relatively low work functions. This negative surface-ionization process has been studied to a lesser extent that positive-ion emission. These studies should be somewhat more difficult to carry out, because the negative-ion flux and the flux of electrons that may be emitted thermally from the surface at the same time would have to be separated and identified.

#### 5.5 SURFACE ELECTRON DENSITY OF STATES

When X-ray photons of energy  $h\nu$  impinge on a solid, electrons are emitted from those occupied electronic states where the electron-binding energies  $E_B$  are less than the energy of the incident photons minus the work function. The kinetic energy  $E_{\rm kin}$  of the emitted so-called photoelectrons is related to the binding energy of electrons in the states they occupied by

$$E_{\rm kin} = h\nu - E_B - \phi \tag{5.18}$$

If the ejection probability is the same for all electron states, the intensity distribution of photoemitted electrons as a function of their kinetic energy provides a true image of the occupied electronic density of states (number of electrons with a given binding energy in the range  $E_B$  to  $E_B + \Delta E$ ). Figure 5.10 shows the electron density of states for nickel and copper determined in this way.

Because the X-ray photons may eject electrons from a depth of over 10 atomic layers, mainly the bulk density of states is obtained in this way. The electron density of states for surface atoms should be different from that in the bulk because the bonding environment for surface atoms is different in their number of nearest neighbors, relaxation or reconstruction, and anisotropy of bonding that could give rise to

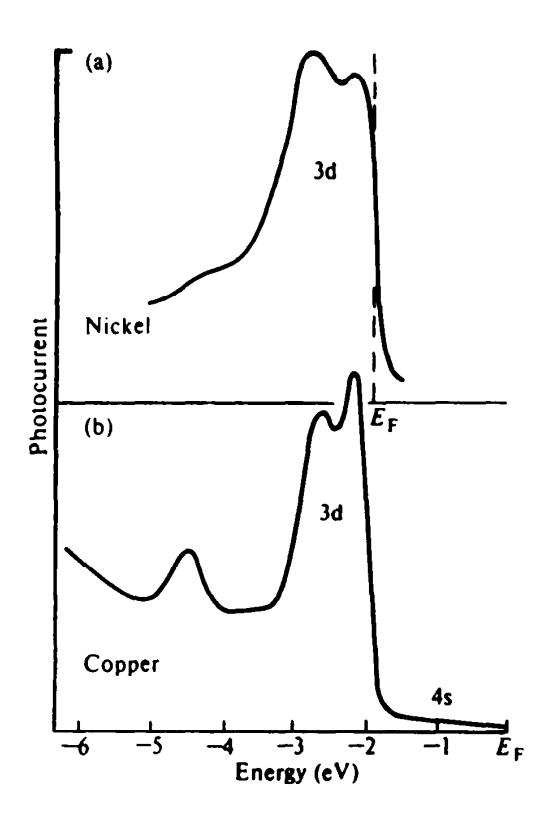


Figure 5.10. Electron density of states for nickel and copper [55].

new electronic states, called *surface states*. It turns out that by observing the photoemitted electrons at near-grazing exit angles or by using lower-energy photons in the ultraviolet range [ $\approx$ 22 eV] (3.5  $\times$  10<sup>-18</sup> J) (ultraviolet photoelectron spectroscopy), the photoemission becomes much more surface-sensitive [6]. Experiments of this type yield the surface electron density of states, which has been found to be narrower than for the bulk, both by experiment and by calculation. In addition, new features, electrons that are localized at surface atoms in bound states, appear due to surface states. Often electrons in these states participate in bonding with adsorbed atoms or molecules. These measurements yield the electronic structure of the surface atoms. Many of the physical and chemical properties of surfaces depend on this property. These include electron transport along the surface, and bonding of atoms and molecules are controlled by the surface electronic structure.

#### 5.6 ELECTRON EXCITATION AT SURFACES

When an electron in an atom or molecule is excited into an unoccupied bound state, it leaves an electron vacancy, or hole, behind. The electron-hole pair thus created exhibits a Coulomb attraction that is modified by the screening of all the other electrons in the system. The same phenomenon occurs when an electron is excited—by light (or electron beam) of appropriate energy—into a bound state above the Fermi level in an semiconductor. The electron-hole pair created in this circumstance is called an *exciton*, and its attractive Coulomb interaction is screened by the static dielectric constant of the solid. There is a finite probability that the exciton may migrate from atom to atom (or molecule to molecule) through the solid before deexcitation, the destruction of the electron-hole pair by recombination, occurs. Exciton

hopping (that is, the correlated migration of the electron-hole pair) has been observed in molecular solids. In semiconductors, the electrons and holes may move independently under the influence of an applied potential that overcomes their screened Coulomb attraction. When electron-hole pairs are created by photoexcitation, photocurrents can be observed that are proportional to the intensity of the photon flux. The deexcitation process leading to electron-hole recombination, whether excited by photons or electrons, is often associated with light emission. The light emission is used in such applications as television screens or light-emitting diodes.

In a metal, the superposition of many electron-hole pairs leads to a wave-like disturbance of the charge density at the surface. This disturbance is called the surface plasmon. Its frequency is related to the bulk plasma frequency  $\omega_b$ : as  $\omega_s = \omega_b/\sqrt{2}$ . The existence of both surface and bulk plasma excitation was detected under conditions of electron-beam or photon excitation, and their corresponding energies are in the range of 5-20 eV (8-32 × 10<sup>-19</sup> J).

#### 5.6.1 Thermal Emission of Electrons from Surfaces

When a metal or an oxide filament is heated in vacuum, electrons boil off its surface. These electrons can be collected on a positive charged plate a short distance away or can be focused by charged plates. This phenomenon is often called *thermionic emission* and is often used to produce electron beams. The electrons that require the least amount of thermal energy to overcome their binding energy in the solid and evaporate are at the top of the valence band. The energy distribution of these electrons can be approximated by a Boltzmann distribution.

$$f(E) \approx \exp\left(-\frac{\phi}{k_B T}\right)$$
 (5.19)

where  $\phi$  is the work function.\* One can compute the flux at energy  $E > \phi + E_F$  of electrons leaving the metal at any one temperature. This value will give us the current density j (A/cm<sup>2</sup>):

$$j\left(\frac{A}{cm^2}\right) = en(E)v_z \tag{5.20}$$

\*Electrons in a solid obey Fermi-Dirac statistics,

$$f(E) = \frac{1}{1 + \exp\left[(E - E_F)/k_BT\right]}$$

where f(E) gives the probability that a state of energy E will be occupied in thermal equilibrium.  $E_F$  is the chemical potential (or Fermi level) and is defined as the energy of the topmost filled electron state at absolute zero temperature. For the high-energy tail of the distribution, we have  $(E - E_F) > k_B T$ . Since, under these conditions, the exponential term is dominant, the unity in the denominator can be neglected, and we have essentially the Boltzmann distribution,

$$f(E) = \exp\left[-(E - E_F)/k_BT\right]$$

		Richardson Constants			
Metal	Temperature (K) for $1.3 \times 10^{-5}$ Pa Vapor Pressure	$(10^{-4} \text{ A/m}^2 \text{K}^2)$	Φ (eV)	$\Phi$ (10 <sup>-19</sup> J)	
Cs	273	160	1.81	2.90	
Ba	580	60	2.11	3.38	
Ni	1270	60	4.1	6.57	
Pt	1650	170	5.4	8.65	
Mo	1970	55	4.15	6.65	
C	2030	48	4.35	6.97	
Ta	2370	60	4.10	6.57	
W	2520	80	4.54	7.27	
Th	1800		2.7	4.33	
Zr	1800		3.1	4.97	

**TABLE 5.7. Thermionic Work Functions of Several Metals** 

where n(E) is the concentration of high-energy electrons,  $v_z$  is their velocity normal to the surface, and e is the unit charge. After integration over the Boltzmann distribution (treating the electrons in the metal as an electron gas) between the limits of E and  $\infty$  in the z direction and between  $-\infty$  and  $\infty$  in the x and y directions, we have

$$j\left(\frac{A}{cm^2}\right) = \frac{1}{2} eN_0 \left(\frac{2k_B T}{\pi m}\right)^{1/2} exp\left(-\frac{\phi}{k_B T}\right)$$
 (5.21)

where m is the electron mass and  $N_0$  is the density of states that gives the number of electron states per unit volume. It is given by  $N_0 = 2(2\pi mk_BT/h^2)^{3/2}$ . Substitution of  $N_0$  into Eq. 5.21 gives

$$j\left(\frac{A}{cm^2}\right) = AT^2 \exp\left(-\frac{\phi}{k_B T}\right) \tag{5.22}$$

where  $A = 4\pi emk_b^2/h^3 = 120 \text{ A/cm}^2\text{K}^2$ . This is the well-known Richardson-Dushman equation.

The electron flux leaving the surface increases with increasing temperature and decreasing work function. Thermionic emission is the method used most frequently to produce electron beams.\* Table 5.7 gives the thermionic work function of several materials. Barium and its compounds (oxide and silicate) and cesium are used most frequently as cold cathodes, since large electron currents may be obtained from their surfaces even at low temperatures because of their work functions.

<sup>\*</sup>More in-depth discussions of the uses of thermionic emission and the experimental variations in cathode emission are given in references [7–11].

# 5.7 ELECTRON EMISSION FROM SURFACES BY INCIDENT ELECTRON OR PHOTON BEAMS

Electron emission from surfaces induced by an electron or photon beam is one of the most successful means of learning about structure, composition, and bonding at surfaces on the atomic level. Electrons can be emitted readily from a solid by incident photons or electrons with energies of the emitted electron greater than the work function (a few electron volts). When electrons are emitted at low kinetic energies, they come only from surface atoms, because electrons emitted from atomic layers under the topmost layer lose their energy by collisions before exiting the surface. Figure 5.11 shows the mean free path of electrons for inelastic scattering in solids as a function of the kinetic energy of the emitted electron. The curve shown in Figure 5.11, which is often called the *universal curve* (because it is applicable to most solids), exhibits a broad minimum in the energy range between 10 and 500 eV (1.6  $\times$  10<sup>-18</sup>  $\rightarrow$  8  $\times$  10<sup>-17</sup> J), with the corresponding mean free paths on the order of 4-20 Å (0.4-2 nm).

Let a monochromatic beam of electrons of energy  $E_p$  (the primary electron beam) strike a solid surface. A typical plot of the number of scattered electrons N(E) as a function of their kinetic energy E is shown in Figure 5.12. The N(E) versus E curve shows a broad peak at low energies, due to secondary electrons created as a result of inelastic collisions between the incident electrons and the electrons bound to the solid. Thus one incident electron may cause the emission of several low-energy electrons from the solid.

Some of the electrons elastically back-scatter with energy  $E_p$ . These electrons will back-diffract from the surface if their de Broglie wavelength,

$$\lambda(\text{nm}) = \sqrt{\frac{1.5}{E(\text{eV})}} \qquad \lambda(\text{Å}) = \sqrt{\frac{150}{E(\text{eV})}}$$

is smaller than or equal to the interatomic distance. This occurs in the 10-500 eV [1.6-80.1  $\times$  10<sup>-18</sup> J] range, corresponding to  $\lambda = 3.9$  Å (0.39 nm) and 0.64 Å (0.064 nm), respectively.

Low-energy electron diffraction (LEED) has proved to be a powerful tool for providing information about periodic surface structures. Small energy losses [in the meV  $(10^{-22} \text{ J})$  range] by the incident electrons provide the energy to excite vibrations and produce vibrational spectra of adsorbed atoms and molecules (high-resolution electron-energy-loss spectroscopy). Energy losses in the 1-20 eV  $(1.6-32 \times 10^{-18} \text{ J})$  range are caused by electronic excitations such as plasma excitation or electron excitation of adsorbed species. Higher-energy electrons cause electron emission from inner shells of surface atoms. The deexcitation processes that follow lead to Auger electron emission and X-ray fluorescence. Both of these processes provide information about surface composition, since the energies of the emitted electrons or photons identify the emitting atom.

Photon beams incident on surfaces induce vibrational excitation of adsorbed molecules at low energies [in the meV ( $\approx 10^{-22}$  J) range]. Photoemission of electrons from the valence band [the 5-30 eV (8-48  $\times$  10<sup>-19</sup> J) range] yields the surface density of electronic states. Photoemission of electrons from inner shells (30-104)

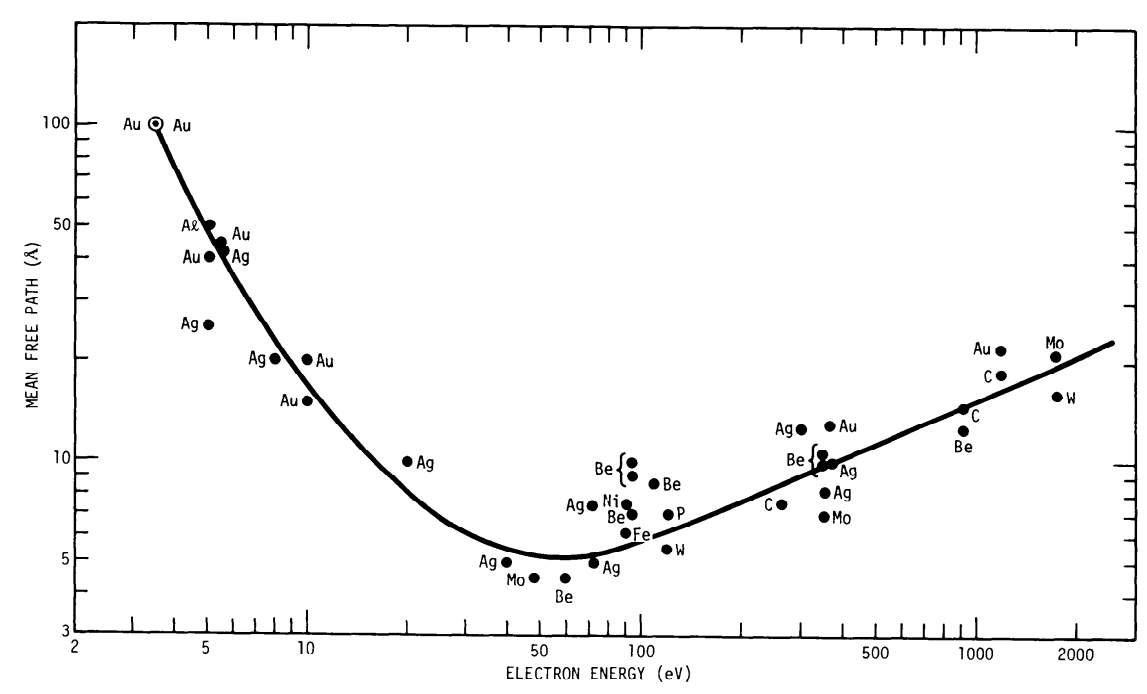


**Figure 5.11.** The mean free path of electrons in different solids as a function of the kinetic energy of the electrons [56].

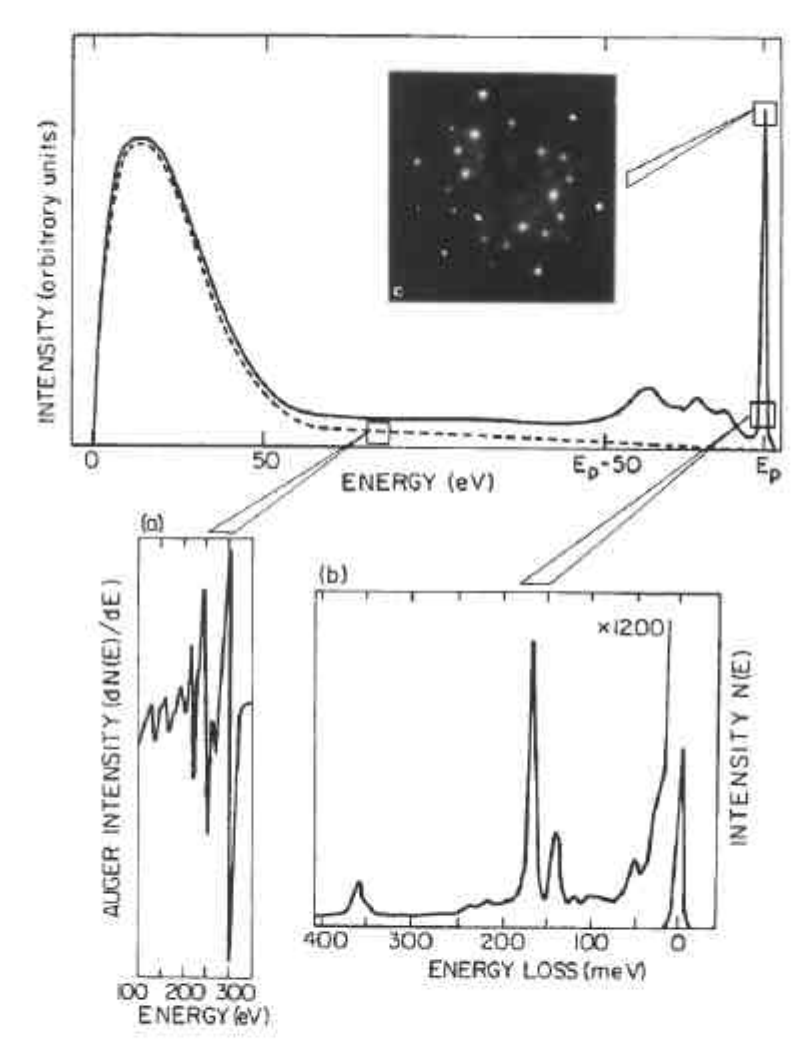


Figure 5.12. Energy distribution of scattered electrons from an ethylene-covered Rh(111) crystal surface at 300 K [57].

eV  $\approx 4.8 \times 10^{-18} = 1.6 \times 10^{-15}$  J) is used in photoelectron spectroscopy to identify the surface composition and the oxidation states of surface atoms. The diffraction of X-ray photoelectrons yields information about surface structure.

Many of the processes that occur during electron (photon)-surface interactions form the foundation of the various techniques of surface analysis. They are described briefly in the list of techniques discussed in Chapter 1. Here we discuss three of the spectroscopies—high-resolution electron-energy-loss spectroscopy, X-ray photo-electron spectroscopy, and Auger electron spectroscopy—because of their prominent roles in surface chemistry.

# 5.7.1 High-Resolution Electron-Energy-Loss Spectroscopy (HREELS)

In HREELS [12–16], an electron beam of 5–20 eV ( $\approx 10^{-19}$  J) energy strikes a solid surface. The back-reflected electrons' energies can be measured with an energy resolution of about 5 meV ( $40~{\rm cm}^{-1} \approx 8 \times 10^{-22}$  J), which is about an order of magnitude better than the energy resolution used in other electron spectroscopies. (This is the reason for the name, although photon spectroscopies have much higher

energy resolutions.) This highly monochromatic beam, upon incidence, excites the various chemical bonds (M—H, M—O, C—H, or C—C, where M is the substrate atom). The frequency modes of these chemical bonds are in the 500-2500 cm<sup>-1</sup> (1-  $5 \times 10^{-20}$  J) range. A typical vibrational spectrum of an organic molecule, o-xylene, on the Rh(111) crystal face is shown in Figure 4.5. The electrons are back-reflected from the surface with energies equal to  $E_{\text{reflected}} = E_{\text{incident}} - E_{\text{vibration}}$ , and they are detected by a suitable energy analyzer. Using HREELS, not only is hydrogen readily detectable at coverages much lower than a monolayer, but also isotope shifts due to different masses of H and D can be observed (Figure 5.13). Adsorbed species with chemical bonds perpendicular to the surface are more readily detectable than adsorbed species with chemical bonds parallel to the surface. The surface sensitivity of this technique is so high ( $\approx 1\%$  of a monolayer) that the structure of the molecules

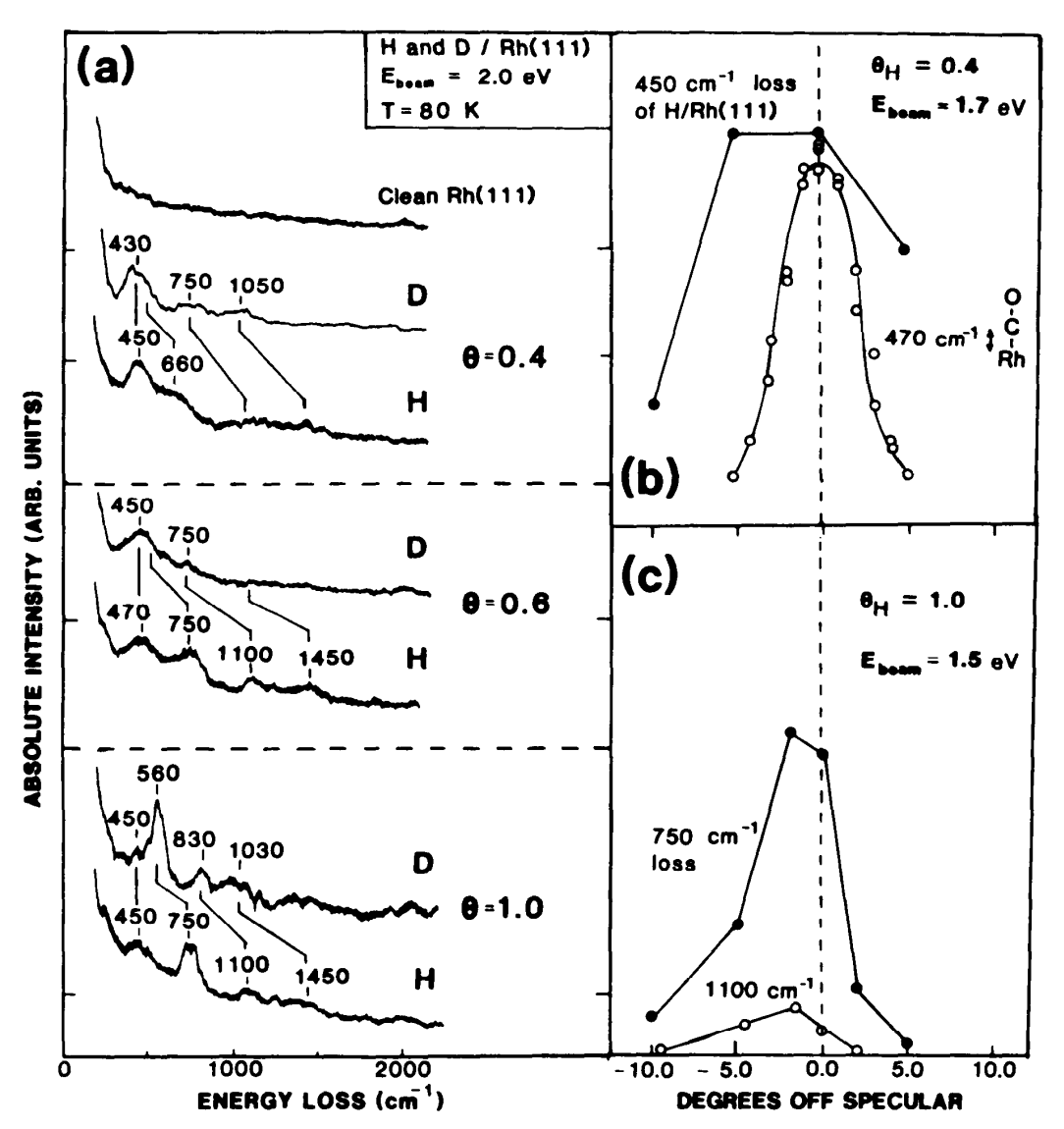


**Figure 5.13.** (a) Vibration spectra of hydrogen and deuterium adsorbed on Rh(111) systems at different coverages at 80 K. The data were taken by HREELS. (b) The angular distribution of the 450-cm<sup>-1</sup> and 470-cm<sup>-1</sup> loss peaks. (c) The angular distribution of the 750-cm<sup>-1</sup> and 1100-cm<sup>-1</sup> loss peaks [58].

adsorbed at the different adsorption sites can be monitored as they fill up the various sites with increasing coverages.

## 5.7.2 X-Ray Photoelectron Spectroscopy (XPS)

XPS [13, 14, 17-25] provides information about elemental surface composition. The principle of photoelectron spectroscopy is the excitation of electrons in an atom or molecule by means of X-rays into vacuum. The ejected photoelectrons have a kinetic energy  $E_{\rm kin}$  equal to

$$E_{\rm kin} \approx h\nu - E_{\rm B} \tag{5.23}$$

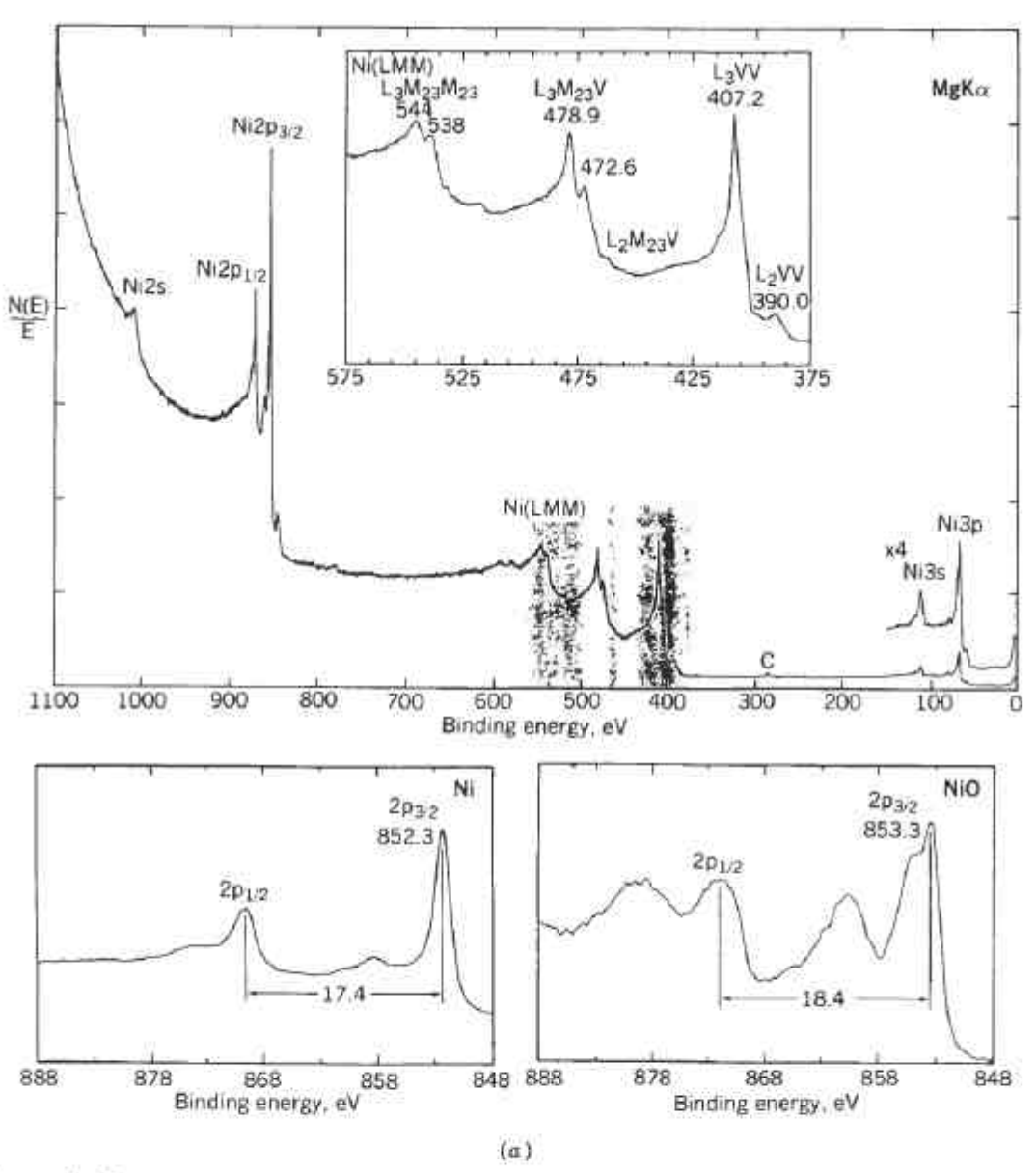


Figure 5.14. Typical XPS spectra from three different transition metals [59]: (a) nickel (nickel oxide is shown for comparison); (b) copper (copper oxide is shown for comparison); (c) zirconium (carbon and oxygen impurity peaks are also shown).

where hv is the energy of the incident X-rays and  $E_B$  is the binding energy of the ejected electron. The X-ray source [26] often consists of an anode of material, usually Al or Mg. The energies of these lines are 1253.6 eV (2 × 10<sup>-16</sup> J) for Mg, with a full width at half-maximum (FWHM) of 0.7 eV (10<sup>-10</sup> J), and 1486.6 eV (2.4 × 10<sup>-16</sup> J) for Al, with an FWHM of 0.85 eV (1.4 × 10<sup>-19</sup> J). Typical XPS spectra are shown in Figure 5.14.

Another frequently used photon source is synchrotron radiation. When high-energy electrons are accelerated to energies of 1 to 6 GeV  $(1.6 \times 10^{-14} \text{ to } 10^{-12} \text{ J})$ , electromagnetic radiation is emitted in the 10 to  $10^4$  eV  $(1.5 \times 10^{-18} \text{ to } 1.6 \times 10^{-15} \text{ J})$  energy range. Continuous radiation in this energy range, which has intensities more than five orders of magnitude higher than a conventional X-ray tube, provides a powerful probe of the electronic structure of atoms and molecules.

Equation 5.23 gives a highly simplified relationship between the kinetic energy

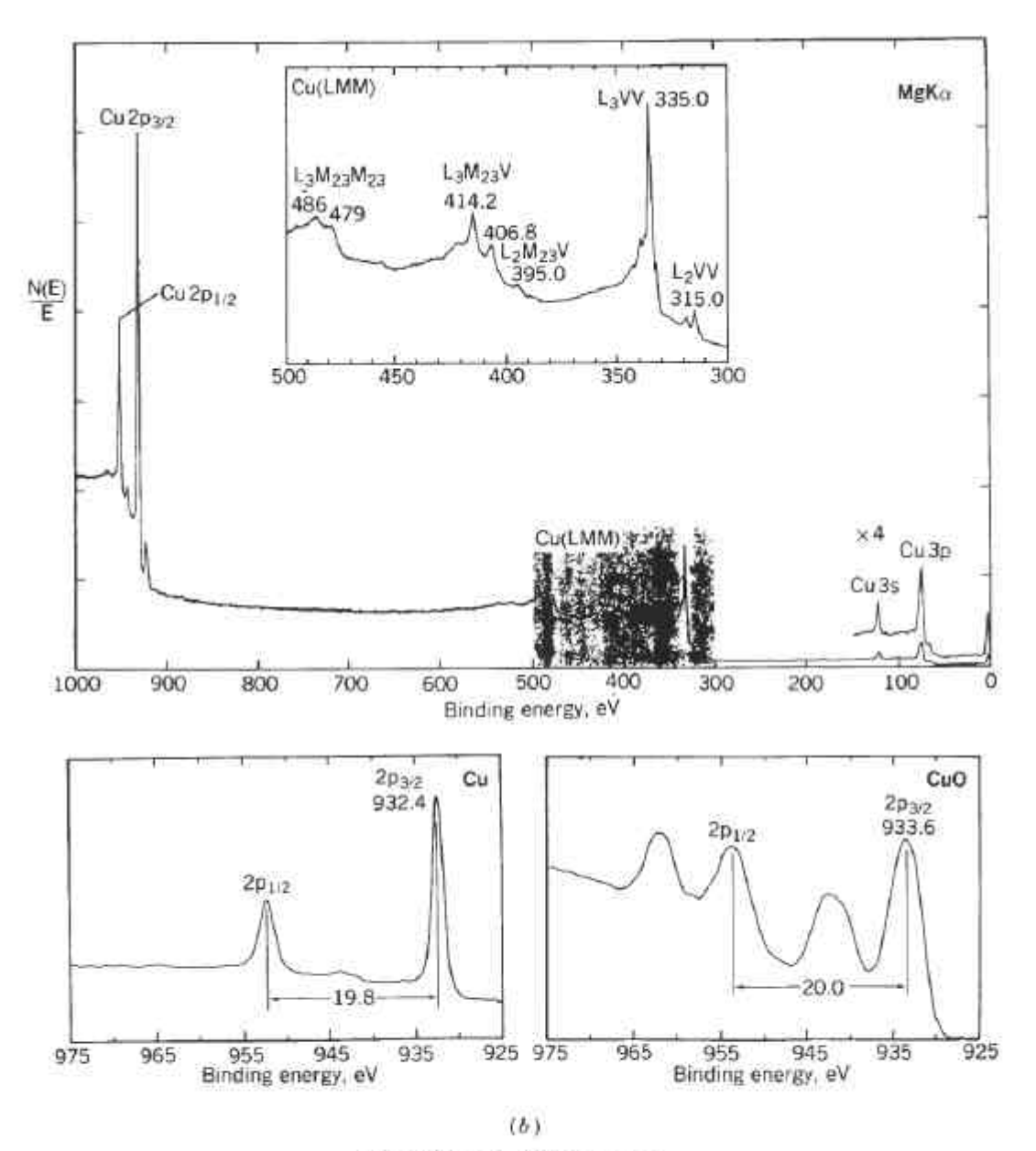


Figure 5.14. (Continued)

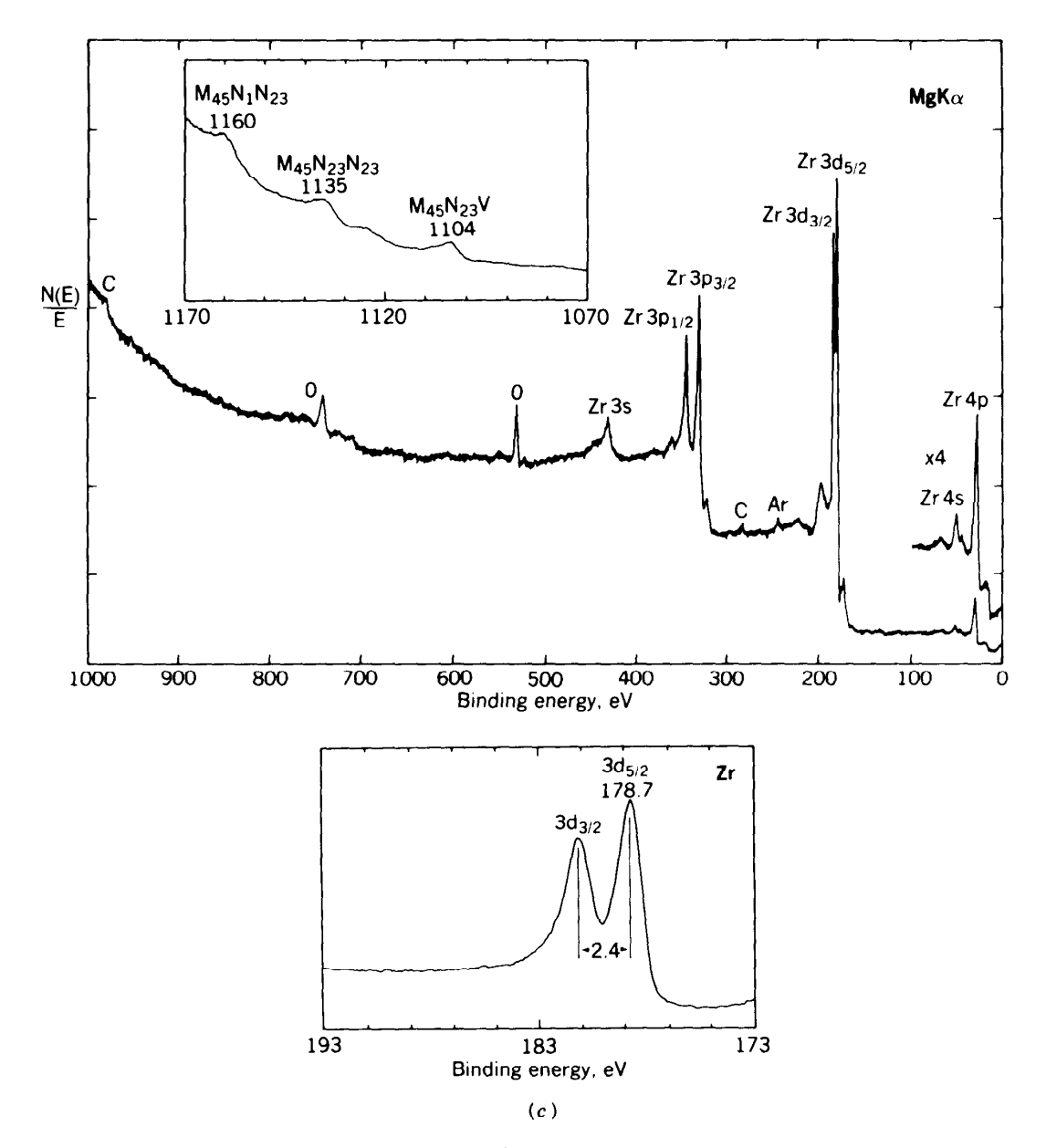


Figure 5.14. (Continued)

 $E_{\rm kin}$  of the emitted photoelectrons and their binding energy. The value of  $E_{\rm kin}$  may be modified by several atomic parameters that are associated with the electron emission process.

One of the most important additional applications of XPS is the determination of the oxidation state of elements at the surface. The electronic binding energies for inner-shell electrons shift as a result of changes in the chemical environment. An example of these shifts can be seen in nitrogen, indicating the photoelectron energy for various chemical environments (Figure 5.15). These energy shifts of the core electrons are closely related to charge transfer in the outer electronic level. The charge redistribution of valence electrons induces changes in the binding energy of the core electrons, so that information on the valence state of the element is readily obtainable. A loss of negative charge (oxidation) is usually accompanied by an increase in the binding energy  $E_B$  of the core electrons.

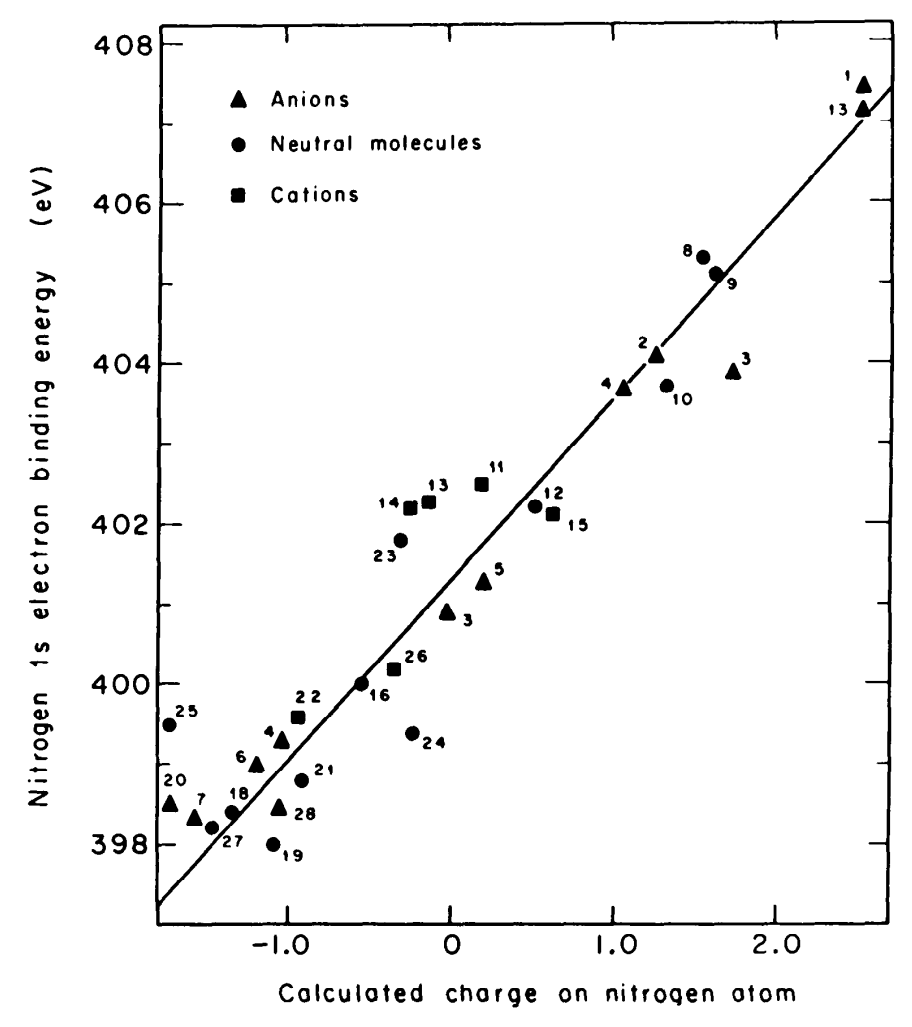


Figure 5.15. The binding energy of nitrogen 1s electrons as a function of the calculated charge on the nitrogen atom in different chemical environments [57].

The surface sensitivity of photoelectron spectroscopy is increased by collecting the emitted electrons that emerge at small angles to the surface plane, as was mentioned before. These electrons must travel a longer distance in the solid, and therefore they are more likely to be absorbed unless they are generated at the surface or in the near surface region.

#### 5.7.3 Auger Electron Spectroscopy (AES)

Auger electron spectroscopy [13, 14, 19-21, 27-38] is suitable for studying the composition of solid and liquid surfaces. Its sensitivity is about 1% of a monolayer, and it may be used with relative ease, compared with several other techniques of electron spectroscopy. When an energetic beam of electrons or X-rays [1000-5000 eV  $(1.6-8 \times 10^{-16} \text{ J})]$  strikes the atoms of a material, electrons which have binding energies less than the incident beam energy may be ejected from the inner atomic level. By this process a singly ionized, excited atom is created. The electron vacancy thus formed is filled by deexcitation of electrons from other electron energy states. The energy released in the resulting electronic transition can be transferred by electrostatic interaction to still another electron in the same atom or in a different atom.

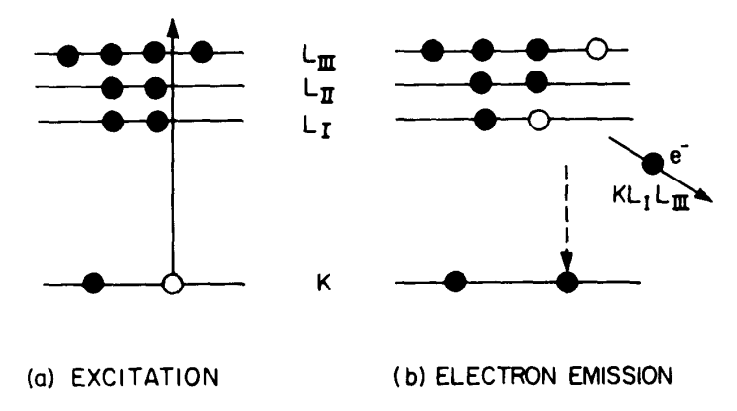


Figure 5.16. Scheme of the Auger electron emission process.

If this electron has a binding energy that is less than the energy transferred to it from the deexcitation of the previous process (which involves filling the deep-lying electron vacancy), it will then be ejected into vacuum, leaving behind a doubly ionized atom. The electron ejected as a result of the deexcitation process is called an *Auger electron*, and its energy is primarily a function of the energy-level separations in the atom. Thus measurement of the Auger electron energy identifies the atom it comes from. These processes are schematically displayed in Figure 5.16.

Most Auger spectroscopy studies of surfaces are carried out for qualitative as well as quantitative surface chemical analysis [39]. Typical Auger spectra from alloy surfaces are shown in Figure 5.17. While the raw experimental data yield the electron intensity as a function of its energy (I versus eV), it is usually displayed as the second derivative of intensity  $d^2I/dV^2$  as a function of electron energy eV. In this way the Auger peaks are readily separated from the background, due to other electron-loss processes that take place simultaneously.

#### 5.8 FIELD ELECTRON EMISSION

When a potential V is applied between a metal tip and a plate, a large electrical field E can be generated at the tip because of its small curvature ( $E \approx V/r$ ). Thus, for  $V = 10^3$  volt and  $r = 10^{-4}$  cm ( $10^{-6}$  m), an electrical field of  $10^7$  volt/cm ( $\approx 10^9$  V/m) can be obtained, large enough to cause field electron emission [13, 14, 19, 21, 30, 40-42]. The applied potential reduces the barrier height, which is represented by the work function in the absence of the electrical field, according to the Fowler-Nordheim equation

$$I = AV^2 \exp\left(-\frac{b\phi^{3/2}}{V}\right) \tag{5.24}$$

where A and b are constants for a given material. One way to observe field electron emission is by using the field electron microscope. A fine tip of radius of  $10^2$  nm  $(10^3 \text{ Å})$  is produced, and a potential of 1-5 kV is applied between it and a plate. (The tip is negatively charged.) The plate is covered with a phosphor that emits light in proportion to the incident electron flux. The space between the tip and the detector

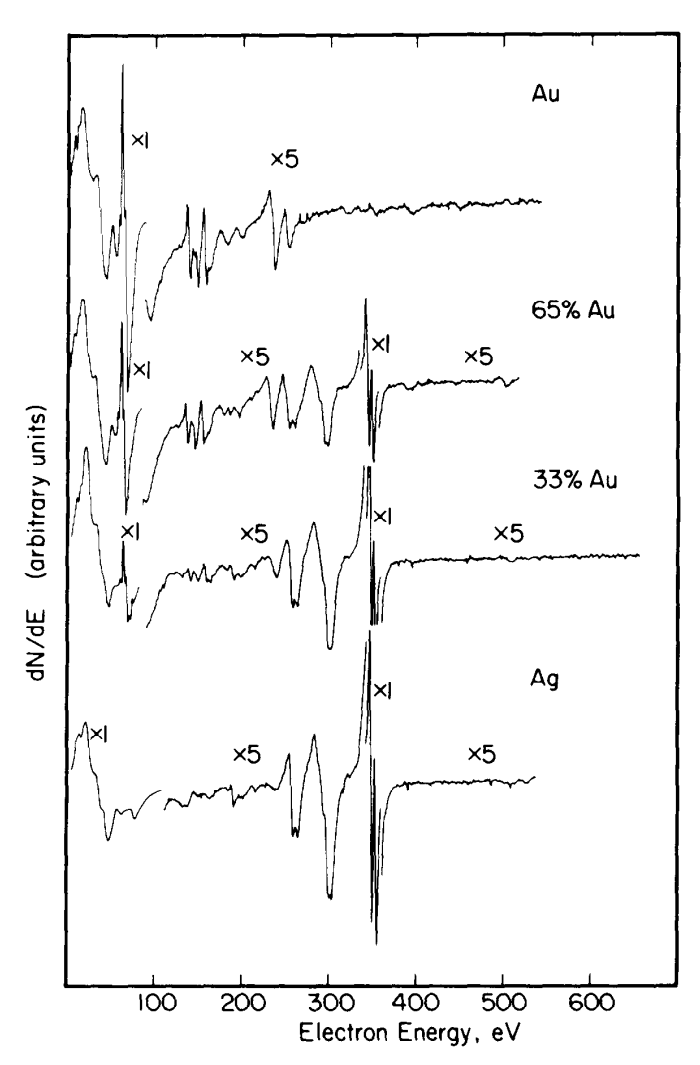


Figure 5.17. Typical AES spectra from pure gold and silver and their alloys [60].

plate is evacuated so that the electron mean free path in the partial vacuum is larger than the size of the apparatus.

#### 5.9 FIELD IONIZATION

The large electrical field at the tip of a field electron microscope can be used to ionize gas atoms that approach it or adsorb on it [13, 14, 19, 21, 30, 40, 42, 43]. If the tip is positively charged in order to repel the positive ions formed, field ionization of an approaching atom occurs at a critical distance X [about 4–8 Å (0.4–0.8 nm)] from the tip, defined by  $X \approx (V_{\text{ion}} - \phi)/E$ , where  $V_{\text{ion}}$  is the ionization potential of the gas atom. The ionization probability depends strongly on the local field variations induced by the atomic structure of the surface. Therefore, field ionization microscopy (FIM) can be used to image the surface. Protruding atoms (adatoms, atoms at steps or kinks) have lower local work functions and therefore generate more ionization than atoms embedded in close-packed atomic planes. Thus, protruding atoms produce individual bright spots on the screen. The imaging of the atomic surface structure of the tip by ions occurs with very little uncertainty in the location of the site from which the ions are emitted, because the ions move very

little tangential to the tip surface, especially at low temperatures ( $T \approx 21$  K is often used for that reason). This small lateral movement allows a spatial resolution of 2-3 Å (0.2-0.3 nm). Small-radius tips are needed to produce the large field required for ionization, but small-radius tips also permit the immense magnification of this microscope, about  $10^7$ -fold.

#### 5.10 ELECTRON TUNNELING

When a sharp tip is brought within 5-10 Å (0.5-1.0 nm) of a surface and a small ( $\approx 10$  volt) potential is applied between the two, quantum tunneling of electrons occurs. This effect produces a tunneling current I, given by the formula

$$I = CV \exp\left(-AVwx\right) \tag{5.25}$$

where C and A are constants, w is the tunnel barrier height, and x is the distance between the tip and the sample surface. (The formula is for one-dimensional tunneling and is an approximation for the tunneling tip.) The tunneling current changes exponentially with the tip-surface distance and can be stabilized by an electronic control unit. The tip can be moved along and perpendicular to the surface by piezo-electric ceramics that extend or contract by the application of suitable voltages (about 1 Å per volt). Measurement of the tunnel current as a function of atomic-scale displacement of the tip along the surface permits imaging of the surface structure.

### 5.10.1 The Scanning Tunneling Microscope (STM)

Electron tunneling and tip motion are the basis of the STM [14, 44-51] (Figure 5.18). Macroscopic tips always have certain whiskers of atomic dimensions due to clusters of atoms that act like minitips. The minitip that happens to be closest to the surface will draw all the tunnel current and will provide the spatial localization required for high-resolution imaging. Typical values for tunnel currents vary from 10

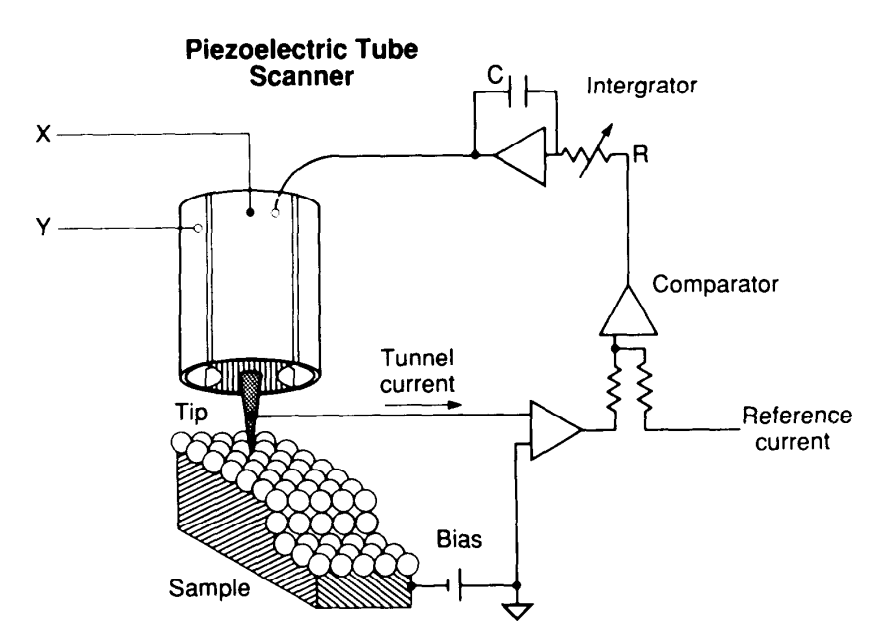


Figure 5.18. Scheme of the scanning tunneling microscope.

pA to 10 nA. An STM picture of a graphite surface at atomic resolution is shown in Figure 2.5.

The STM may be operated by moving it along the surface in the constant-height mode or in the constant-current mode (topographic mode). In the constant-height mode, the height of the tip is kept constant, and the variation in current is measured (the closer the distance, the greater the current crossing the gap). In the topographic mode, the tunneling current is kept constant by moving the tip in and out, always at a constant distance from the surface. By oscillating the tip the tunnel current can be modulated (dI/dx) to image the local barrier height. Investigations of the applied voltage dependence of the tunnel current should provide information about the local electron density of states.

Electron tunneling spectroscopy applied in a different experimental configuration can yield the vibrational structure of adsorbates. For example, by adsorbing a monolayer of molecules at an aluminum oxide-lead interface, the vibrational spectrum of benzoic acid was obtained by plotting  $d^2V/dI^2$ , the second derivative of the applied voltage with respect to the tunnel current, versus the applied voltage V. The result is shown in Figure 5.19. The experiment was performed at 4.2 K.

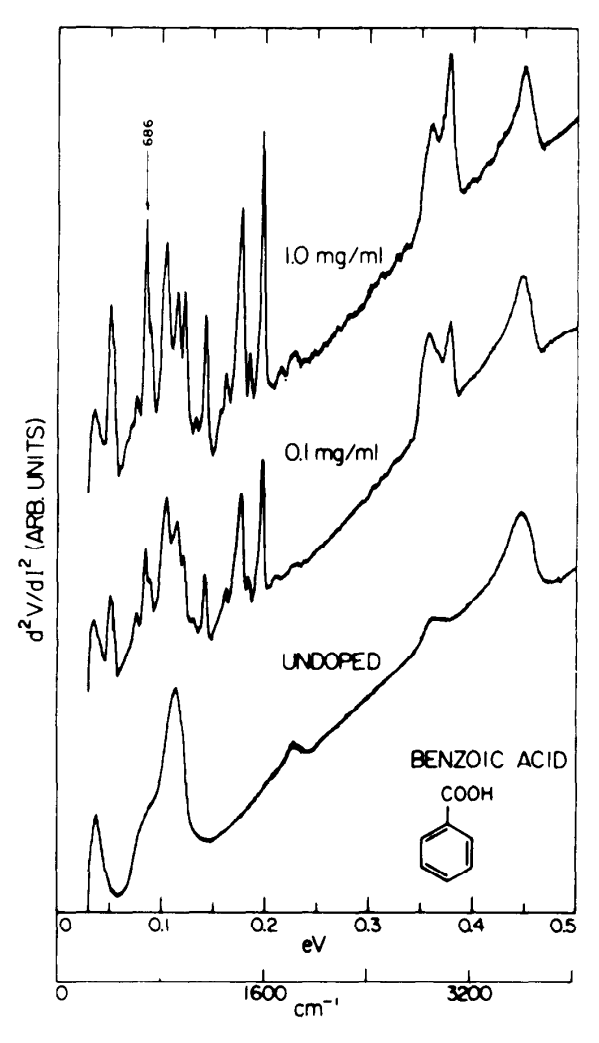


Figure 5.19. Electron tunneling spectra from aluminum oxide-lead junctions with benzoic acid adsorbate. Acid solution strength are indicated. The junction spectrum without the adsorbate is included for comparison [61].

#### 5.11 SUMMARY AND CONCEPTS

- The discontinuity and change of dimensionality (from three to two dimensions) at solid-vacuum, solid-gas, and solid-liquid interfaces gives rise to electron redistribution. These effects result in surface space charges, surface electronic states, and work functions that are altered by changes of surface structure and adsorption.
- Charge transfer at the interface may control (a) electron transport near the surface and (b) the nature of adsorption.
- Surface ionization of adsorbates can take place under appropriate circumstances.
- Excited surface-atom vibrations induced by incident electrons have many applications in surface science.
- Electron emission from the valence band induced thermally by photons or by other electrons also has many applications in surface studies.
- The emission of inner-shell electrons from surface atoms is used for chemical analysis and determination of oxidation states.
- Electric-field-induced electron emission or tunneling and ionization of atoms at sharp tips are used to image surface atoms.

#### 5.12 PROBLEMS

- 5.1 Milk and latex paint are two colloid systems. Describe the reasons for their stability [62].
- When potassium is deposited on the (111) crystal face of rhodium, the work function of the metal decreases markedly. At 20% monolayer coverage, the work function change attains its minimum value of -1.8 eV. If the Rh-K interatomic distance is 1.2 Å, what is the charge transfer at the adsorption site of the alkali metal?
- 5.3 (a) Calculate the electron flux from a hot tungsten filament at 2200 K. (b) At what temperature would you need to operate a BaO cathode to obtain the same current? Assume  $\phi_{\text{BaO}} = 1.1 \text{ eV}$  and  $A_{\text{BaO}} = 3.5 \text{ mA/cm}^2\text{K}^2$ .
- \*5.4 Low-energy (5-15 eV) incident electrons can excite the vibrational modes of surface atoms and adsorbed molecules. Describe what has been learned about the (a) bonding of hydrogen atoms on rhodium and tungsten metal surfaces [63-65] and (b) the bonding of CO on rhodium and nickel [66, 67]. Discuss the meaning of dipole and impact electron scattering.
- \*\*5.5 What is the Helmholtz layer at the solid-liquid interface? Discuss the experimental evidence for its existence [68-71].
- \*\*5.6 The contact potential that develops at semiconductor-oxide/metal interfaces dramatically alters the transport of the electrons in the two directions (oxide to metal and metal to oxide). Describe how the current varies as a function in the two directions. Discuss different applications of this phenomenon [72].

- \*\*5.7 The distribution of the space charge can be calculated along the surface of an electrode of a given shape by solving the Poisson equation using appropriate boundary conditions. Review the literature and discuss how the shape of an electrode alters the space charge layer [73].
- \*\*5.8 Gas adsorption changes the electrical conductivity of oxide semiconductor thin films [2,3]. How is this phenomenon utilized to detect methane or carbon monoxide? How would charge transfer to the substrate affect the heat of adsorption of an organic molecule, and how would it affect that of oxygen and nitrogen? Could you use this phenomenon for the separation of O<sub>2</sub> and N<sub>2</sub> in air?
- \*\*5.9 Discuss the principles of Fourier transform infrared spectroscopy and nonlinear laser optics [74, 75], and of second harmonic and sum frequency generation. Compare the relative advantages of both techniques for the study of the bonding, orientation, and location of adsorbed molecules either on metal or on insulator surfaces.
- \*\*5.10 Xerography is one of the dominant methods of producing copies of written material. Describe its principle of operation [76, 77]. How are colored copies made?

#### REFERENCES

- [1] R.L. Whetten, D.M. Cox, D.J. Trevor, and A. Kaldor. Advances in Research on Clusters of Transition Metal Atoms. *Surf. Sci.* **156**:8 (1985).
- [2] M.J. Madou and S.R. Morrison. Chemical Sensing with Solid State Devices. Academic Press, New York, 1989.
- [3] T. Takeuchi. Oxygen Sensors. Sensors and Actuators 14:109 (1988).
- [4] M. Kaminsky. Atomic and Ionic Impact Phenomena on Metal Surfaces. Academic Press, New York, 1965.
- [5] M.D. Scheer and J. Fine. Positive and Negative Self-Surface Ionization of Tungsten and Rhenium. J. Chem. Phys. 46:3998 (1967).
- [6] A. Zangwill. *Physics at Surfaces*. Cambridge University Press, New York, 1988.
- [7] S. Dushman. Scientific Foundations of Vacuum Technique, 2nd edition. John Wiley & Sons, New York, 1962. Revised by the General Electric Research Staff, J.M. Lafferty, editor.
- [8] L.M. Field. High Current Electron Guns. Rev. Mod. Phys. 18:353 (1946).
- [9] J.P. Blewett. The Properties of Oxide-Coated Cathodes. I. J. Appl. Phys. 10:668 (1939).
- [10] J.P. Blewett. The Properties of Oxide-Coated Cathodes. II. J. Appl. Phys. 10:831 (1939).
- [11] S. Dushman. Thermionic Emission. Rev. Mod. Phys. 2:281 (1930).
- [12] W. Ho. High Resolution Electron Energy Loss Spectroscopy. In: B.W. Rossiter and R.C. Baetzold, editors, *Investigations of Surfaces and Interfaces*, *Part A. Physical Methods of Chemistry*, Volume 9A, 2nd edition. John Wiley & Sons, New York, 1993.
- [13] D.P. Woodruff and T.A. Delchar. *Modern Techniques of Surface Science. Cambridge Solid State Science Series*. Cambridge University Press, New York, 1986.

- [14] J.B. Hudson. Surface Science: An Introduction. Butterworth-Heinemann, New York, 1992.
- [15] J.L. Erskine. High Resolution Electron Energy Loss Spectroscopy. In: J.E. Greene, editor, *Critical Reviews in Solid State and Material Sciences*, Volume 13. CRC Press, Boca Raton, FL, 1987.
- [16] J.J. Pireaux, P.A. Thiry, R. Sporken, and R. Caudano. Analysis of Semiconductors and Insulators by High Resolution Electron Energy Loss Spectroscopy—Prospects for Quantification. *Surf. Interface Anal.* 15:189 (1990).
- [17] J.F. Moulder, W.F. Stickle, P.E. Sobol, and K.D. Bomben. *Handbook of X-Ray Photoelectron Spectroscopy*. Perkin Elmer, Eden Prairie, MN, 1992.
- [18] M.H. Kibel. X-Ray Photoelectron Spectroscopy. In: D.J. O'Conner, B.A. Sexton, and R. St. C. Smart, editors, *Surface Analysis Methods in Materials Science. Springer Series in Surface Sciences*, Volume 23. Springer-Verlag, Berlin, 1992.
- [19] M.J. Higatsberger. Solid Surfaces Analysis. In: C. Marton, editor, *Advances in Electronics and Electron Physics*, Volume 56. Academic Press, New York, 1981.
- [20] R.L. Park. Core-Level Spectroscopies. In: R.L. Park and M.G. Lagally, editors, *Solid State Physics: Surfaces. Methods of Experimental Physics*, Volume 22. Academic Press, New York, 1985.
- [21] M. Prutton. Surface Physics. Oxford University Press, New York, 1975.
- [22] D.T. Clark. Structure, Bonding, and Reactivity of Polymer Surfaces Studies by Means of ESCA. In: R. Vanselow, editor, *Chemistry and Physics of Solid Surfaces*, Volume 2. CRC Press, Cleveland, OH, 1979.
- [23] D. Briggs. Analytical Applications of XPS. In: C.R. Brundle and A.D. Baker, editors, *Electron Spectroscopy: Theory, Techniques and Applications*, Volume 3. Academic Press, New York, 1979.
- [24] C.D. Wagner, W.M. Riggs, L.E. Davis, J.F. Moulder, and G.E. Muilenberg, editors. Handbook of X-Ray Photoelectron Spectroscopy. Perkin Elmer, Eden Prairie, MN, 1978.
- [25] W.M. Riggs and M.J. Parker. Surface Analysis by X-Ray Photoelectron Spectroscopy. In: A.W. Czanderna, editor, *Methods of Surface Analysis. Methods and Phenomena: Their Applications in Science and Technology*, Volume 1. Elsevier, New York, 1975.
- [26] P.K. Ghosh. *Introduction to Photoelectron Spectroscopy. Chemical Analysis*, Volume 67. John Wiley & Sons, New York, 1983.
- [27] R. Browning. Auger Spectroscopy and Scanning Auger Microscopy. In: D.J. O'Conner, B.A. Sexton, and R. St. C. Smart, editors, *Surface Analysis Methods in Materials Science*. Springer Series in Surface Sciences, Volume 23. Springer-Verlag, Berlin, 1992.
- [28] L.E. Davis, N.C. MacDonald, P.W. Palmberg, G.E. Riach, and R.E. Weber. *Hand-book of Auger Electron Spectroscopy*. Perkin Elmer, Eden Prairie, MN, 1978.
- [29] B.V. King. Sputter Depth Profiling. In: D.J. O'Conner, B.A. Sexton, and R. St. C. Smart, editors, Surface Analysis Methods in Materials Science. Springer Series in Surface Sciences, Volume 23. Springer-Verlag, Berlin, 1992.
- [30] R.P.H. Gasser. An Introduction to Chemisorption and Catalysis by Metals. Oxford University Press, New York, 1985.
- [31] R. Weissmann and K. Müller. Auger Electron Spectroscopy—A Local Probe for Solid Surfaces. Surf. Sci. Rep. 1:251 (1981).
- [32] G. Ertl and J. Küpper. Low Energy Electrons and Surface Chemistry. VCH, New York, 1985.

- [33] J. Kirschner. Polarized Electrons at Surfaces. In: G. Höhler, editor, *Springer Tracts in Modern Physics*, Volume 106. Springer-Verlag, New York, 1985.
- [34] G.E. McGuire and P.H. Holloway. Applications of Auger Spectroscopy in Materials Analysis. In: C.R. Brundle and A.D. Baker, editors, *Electron Spectroscopy: Theory, Techniques and Applications*, Volume 4. Academic Press, New York, 1981.
- [35] J.C. Fuggle. High Resolution Auger Spectroscopy of Solids and Surfaces. In: C.R. Brundle and A.D. Baker, editors, *Electron Spectroscopy: Theory, Techniques and Applications*, Volume 4. Academic Press, New York, 1981.
- [36] C.C. Chang. Analytical Auger Electron Spectroscopy. In: P.F. Kane and G.B. Larrabee, editors, *Characterization of Solid Surfaces*. Plenum Press, New York, 1974.
- [37] P.M. Hall and J.M. Morabito. Compositional Depth Profiling by Auger Electron Spectroscopy. In: R. Vanselow, editor, *Chemistry and Physics of Solid Surfaces*, Volume 2. CRC Press, Cleveland, OH, 1979.
- [38] A. Joshi, L.E. Davis, and P.W. Palmberg. Auger Electron Spectroscopy. In: A.W. Czanderna, editor, *Methods of Surface Analysis*, *Methods and Phenomena: Their Applications in Science and Technology*, Volume 1. Elsevier, New York, 1975.
- [39] J.M. Slaughter, W. Weber, G. Güntherot, and C.M. Falco. Quantitative Auger and XPS Analysis of Thin Films. *MRS Bull.* **December:**39 (1992).
- [40] G.A. Somorjai and M.A. Van Hove. Adsorbed Monolayers on Solid Surfaces. In: J.D. Dunitz, J.B. Goodenough, P. Hemmerich, J.A. Albers, C.K. Jørgensen, J.B. Neilands, D. Reinen, and R.J.P. Williams, editors, *Structure and Bonding*, Volume 38. Springer-Verlag, New York, 1979.
- [41] R. Gomer. Recent Applications of Field Emission Microscopy. In: R. Vanselow, editor, *Chemistry and Physics of Solid Surfaces*, Volume 2. CRC Press, Cleveland, OH, 1979.
- [42] J.A. Panitz. High-Field Techniques. In: R.L. Park and M.G. Lagally, editors, *Solid State Physics: Surfaces. Methods of Experimental Physics*, Volume 22. Academic Press, New York, 1985.
- [43] G. Ehrlich. Wandering Surface Atoms and the Field Ion Microscope. *Phys. Today* **June:**44 (1981).
- [44] A.L. de Lozanne. Scanning Tunneling Microscopy. In: B.W. Rossiter and R.C. Baetzold, editors, *Investigations of Surfaces and Interfaces, Part A. Physical Methods of Chemistry*, Volume 9A, 2nd edition, John Wiley & Sons, New York, 1993.
- [45] B.A. Sexton. Scanning Tunneling Microscopy. In: D.J. O'Conner, B.A. Sexton, and R. St. C. Smart, editors, *Surface Analysis Methods in Materials Science. Springer Series in Surface Sciences*, Volume 23. Springer-Verlag, Berlin, 1992.
- [46] H.J. Günterodt and R. Wiesendanger, editors. Scanning Tunneling Microscopy I: General Principles and Applications to Clean and Adsorbate Covered Surfaces. Springer Series in Surface Sciences, Volume 20. Springer-Verlag, Berlin, 1992.
- [47] P.K. Hansma, V.B. Elings, O. Marti, and C.E. Bracker. Scanning Tunneling Microscopy and Atomic Force Microscopy: Application to Biology and Technology. *Science* 242:157 (1988).
- [48] L.E.C. van de Leemput and H. van Kempen. Scanning Tunneling Microscopy. *Rep. Prog. Phys.* **55**:1165 (1992).
- [49] M. Tsukada, K. Kobayashi, N. Isshiki, and H. Kagashima. First-Principles Theory of Scanning Tunneling Microscopy. *Surf. Sci. Rep.* 13:265 (1991).
- [50] F. Ogletree and M. Salmerón. Scanning Tunneling Microscopy and the Atomic Structure of Solid Surfaces. *Prog. Solid State Chem.* **20:**235 (1990).
- [51] G. Binnig and H. Rohrer. Scanning Tunneling Microscopy—from Birth to Adolescence. *Rev. Mod. Phys.* **59:**615 (1987).

- [52] K. Besocke, B. Krahl-Urban, and H. Wagner. Dipole Moments Associated with Edge Atoms; a Comparative Study on Stepped Pt, Au, and W Surfaces. *Surf. Sci.* **68:**39 (1977).
- [53] R. Miranda, S. Daiser, K. Wandelt, and G. Ertl. Thermodynamics of Xenon Adsorption on Pd(s)[8(100) × (110)]: From Steps to Multilayers. *Surf. Sci.* 131:61 (1983).
- [54] C.M. Mate, C.T. Kao, and G.A. Somorjai. Carbon Monoxide Induced Ordering of Adsorbates on the Rh(111) Crystal Surface: Importance of Surface Dipole Moments. *Surf. Sci.* **206**:145 (1988).
- [55] J.B. Pendry. Electron Emission from Solids. In: B. Feuerbacher, B. Fitton, and R.F. Willis, editors, *Photoemission and the Electronic Properties of Surfaces*. Wiley-Interscience, New York, 1978.
- [56] G.A. Somorjai. *Chemistry in Two Dimensions: Surfaces*. Cornell University Press, Ithaca, NY, 1981.
- [57] S.R. Bare and G.A. Somorjai. Surface Chemistry. In: R.A. Meyers, editor, *Encyclopedia of Physical Science and Technology*. Academic Press, New York, 1987.
- [58] C.M. Mate. A Molecular Surface Science Study of the Structure of Adsorbates on Surfaces: Importance to Lubrication. Ph.D. thesis, University of California, Berkeley, 1986.
- [59] C.D. Wagner, W.M. Riggs, L.E. Davis, J.F. Moulder, and G.E. Muilenberg, editors. Handbook of X-Ray Photoelectron Spectroscopy. Perkin Elmer, Eden Prairie, MN, 1978.
- [60] S.H. Overbury and G.A. Somorjai. The Surface Composition of the Silver-Gold System by Auger Electron Spectroscopy. *Surf. Sci.* **55:**209 (1976).
- [61] J.D. Langan and P.K. Hansma. Can the Concentration of Surface Species be Measured with Inelastic Electron Tunneling? Surf. Sci. 52:211 (1975).
- [62] P.C. Hiemenz. *Principles of Colloid and Surface Chemistry*, 2nd edition. Marcel Dekker, New York, 1986.
- [63] C.M. Mate and G.A. Somorjai. Delocalized Quantum Nature of Hydrogen Adsorbed on the Rh(111) Crystal Surface. *Phys. Rev. B* **34:**7417 (1986).
- [64] R.F. Willis, W. Ho, and E.W. Plummer. Vibrational Excitation of Hydrogenic Modes on Tungsten by Angle Dependent Electron Energy Loss Spectrometry. *Surf. Sci.* **80:**593 (1979).
- [65] H. Froitzheim, H. Ibach, and S. Lehwald. Surface Sites of H on W(100). *Phys. Rev. Lett.* 36:1549 (1976).
- [66] C.M. Mate and G.A. Somorjai. Carbon Monoxide Induced Ordering of Benzene on Pt(111) and Rh(111) Crystal Surfaces. Surf. Sci. 160:542 (1985).
- [67] W. Erley, H. Wagner, and H. Ibach. Adsorption Sites and Long Range Order—Vibrational Spectra for CO on Ni(111). Surf. Sci. 80:612 (1979).
- [68] J.K. Sass, N.V. Richardson, H. Neff, and D.K. Roe. Towards Model Systems for the Helmholtz Layer: Coadsorption of Water and Bromine on Cu(100). *Chem. Phys. Lett.* 73:209 (1980).
- [69] W.N. Hansen, C.L. Wang, and T.W. Humphries. Electrode Emersion and the Double Layer. J. Electroanal. Chem. Interfacial Electrochem. 90:137 (1978).
- [70] W.J. Anderson and W.N. Hansen. Observing the Electrochemical Interphase via Electrode Conductance. *Electroanal. Chem. Interfacial Electrochem.* **43:**329 (1973).
- [71] R.S. Perkins and T.N. Andersen. Potentials of Zero Charge of Electrodes. In: J. O'M. Bockris and B.E. Conway, editors, *Modern Aspects of Electrochemistry*, Volume 5. Plenum Press, New York, 1969.

- [72] C.A. Wert and R.M. Thomson. *Physics of Solids*, 2nd edition. McGraw-Hill, New York, 1970.
- [73] R.N. Adams. Electrochemistry at Solid Electrodes. Marcel Dekker, New York, 1969.
- [74] Y.R. Shen. *The Principles of Non-Linear Optics*. John Wiley & Sons, New York, 1984.
- [75] A. Yariv. Quantum Electronics, 3rd edition. John Wiley & Sons, New York, 1989.
- [76] D.M. Burland and L.B. Schein. Physics of Electrophotography. *Phys. Today* May:46 (1986).
- [77] E.M. Williams. *The Physics and Technology of Xerographic Processes*. John Wiley & Sons, New York, 1984.